

General Disclaimer

One or more of the Following Statements may affect this Document

- This document has been reproduced from the best copy furnished by the organizational source. It is being released in the interest of making available as much information as possible.
- This document may contain data, which exceeds the sheet parameters. It was furnished in this condition by the organizational source and is the best copy available.
- This document may contain tone-on-tone or color graphs, charts and/or pictures, which have been reproduced in black and white.
- This document is paginated as submitted by the original source.
- Portions of this document are not fully legible due to the historical nature of some of the material. However, it is the best reproduction available from the original submission.

CR 86342

FILM STUDY FOR A STAR CORRELATOR

by C. E. Thomas and W. D. Hall

February 1970

Final report

Distribution of this report is provided in the interest of information exchange and should not be construed as endorsement by NASA of the material presented. Responsibility for the contents resides with the organization that prepared it.

Prepared Under Contract No. NAS 12-2212 by

THE KMS TECHNOLOGY CENTER

7810 Burnet Avenue

Van Nuys, California 91405

Electronics Research Center

NATIONAL AERONAUTICS AND SPACE ADMINISTRATION

Cambridge, Massachusetts

N70-25914

FACILITY FORM 802

(ACCESSION NUMBER)

130

(PAGE)

NASA CR # 86342

(NASA CR OR TRACK NUMBER)

(THRU)

1

(CODE)

14

(CATEGORY)

CR 86342

FILM STUDY FOR A STAR CORRELATOR

by C. E. Thomas and W. D. Hall

February 1970

final report

Distribution of this report is provided in the interest of information exchange and should not be construed as endorsement by NASA of the material presented. Responsibility for the contents resides with the organization that prepared it.

Prepared Under Contract No. NAS 12-2212 by

THE KMS TECHNOLOGY CENTER

7810 Burnet Avenue

Van Nuys, California 91405

Electronics Research Center

NATIONAL AERONAUTICS AND SPACE ADMINISTRATION

Cambridge, Massachusetts

N70-25914

FACILITY FORM 602

(ACCESSION NUMBER)

122

(PAGES)

NASA CR # 86342

(NASA CR OR TMX OR AD NUMBER)

(THRU)

1

(CODE)

14

(CATEGORY)

FILM STUDY FOR A STAR CORRELATOR

by C. E. Thomas and W. D. Hall

February 1970

Prepared Under Contract No. NAS 12-2212 by

THE KMS TECHNOLOGY CENTER

7810 Burnet Avenue

Van Nuys, California 91405

Electronics Research Center

NATIONAL AERONAUTICS AND SPACE ADMINISTRATION

Cambridge, Massachusetts

PRECEDING PAGE BLANK NOT FILMED.

ACKNOWLEDGMENTS: We wish to thank personnel of the Eastman Kodak Company, the 3M Company, Mark Systems, and Photohorizons for supplying data on their films. Special credit is due Photohorizons who supplied equipment to process their free Radical film and also processed several films in their own laboratory.

James N. Hallock
Technical Monitor
NAS 12-2213
Electronics Research Center
565 Technology Square
Cambridge, Massachusetts 02139

Requests for copies of this report should be referred to:

NASA Scientific and Technical
Information Facility
P. O. Box 33
College Park, Maryland 20740

FORWORD

This work was performed at The KMS Technology Center under the direction of Mr. C. E. Thomas. Mr. Thomas is solely responsible for the film study portion of this report, and will use some of this data as part of his PhD thesis from the University of Michigan. The image intensifier investigation was performed by Dr. William D. Hall.

TABLE OF CONTENTS

| <u>Section</u> | <u>Page</u> |
|--|-------------|
| 1.0 INTRODUCTION..... | 1 |
| 2.0 SUMMARY OF INVESTIGATIONS..... | 2 |
| 2.1 Summary Comparison of Film Characteristics | 2 |
| 2.2 Summary of Image Intensification Investigation | 7 |
| 2.3 Summary of Star Image Smearing Study..... | 11 |
| 3.0 DETAILED DESCRIPTION OF FILM INVESTIGATIONS... | 12 |
| 3.1 Description of Unconventional Films Investigated ... | 14 |
| 3.1.1 Free-Radical Film..... | 14 |
| 3.1.2 Dry Silver Film | 15 |
| 3.1.3 BIMAT Transfer Films..... | 16 |
| 3.2 Description of the Film Measurements Equipment... | 18 |
| 3.2.1 Exposure Station | 18 |
| 3.2.1.1 The Exposing Light Source..... | 19 |
| 3.2.1.2 The Exposure Timing System..... | 22 |
| 3.2.3 The T_A -E Curves | 23 |
| 3.2.4 Film Noise Spectra | 24 |
| 3.3 Detailed Results of the Measurements Program | 31 |
| 3.3.1 Amplitude Transmission Versus Exposure Curves | 31 |
| 3.3.1.1 Free Radical T_A -E Curves..... | 31 |
| 3.3.1.2 Dry Silver T_A -E Curve..... | 31 |
| 3.3.1.3 BIMAT Processed T_A -E Curves..... | 34 |
| 3.3.2 Film Noise Spectra..... | 37 |
| 3.4 Summary Evaluation of Rapidly Processed Films.... | 47 |
| 3.5 Recommended Future Film Study Work..... | 47 |
| 4.0 INTRODUCTION TO IMAGE INTENSIFIERS | 51 |
| 4.1 Fiber-Coupled Double-Stage Image Intensifier..... | 54 |

TABLE OF CONTENTS
(continued)

| <u>Section</u> | <u>Page</u> |
|--|-------------|
| 4.1.1 Theoretical Discussion of Flux Gain | 54 |
| 4.1.2 Fiber-Optical Coupler Efficiency..... | 55 |
| 4.1.3 Gain of Fiber Coupled Image Intensifiers..... | 59 |
| 4.1.4 Theoretical Discussion of Paraxial..... Device Resolution | 61 |
| 4.1.5 Device and Quantum Noise Limitations..... | 65 |
| 4.2 Continuous Channel Multiplier Plates..... | 70 |
| 4.2.1 Theory of Operations..... | 70 |
| 4.2.2 Performance of Channel Plate Amplifiers..... | 71 |
| 4.3 Direct Electronographic Intensification..... | 73 |
| 4.3.1 The Lallemand Electronographic Intensifier..... | 73 |
| 4.3.2 A Modified Electronographic Xerographic Image Intensification System..... | 76 |
| 5.0 SYSTEM CONSIDERATIONS..... | 77 |
| 5.1 Optimum Sensitivity..... | 77 |
| 5.2 Noise Matching to Film..... | 80 |
| 5.3 Summary of Image Intensifier Investigation..... | 84 |
| 6.0 EFFECTS OF IMAGE SMEARING DUE TO SPACECRAFT ROTATION | 86 |
| 6.1 The Stationary Spacecraft Exposure Time..... | 86 |
| 6.2 The Maximum Exposure Due to Spacecraft Rotation | 89 |
| 6.3 Increased Sensitivity by Smearred Image Integration | 90 |
| <u>APPENDIX A</u> | |
| Photometric-Radiant Conversions..... | 100 |

TABLE OF CONTENTS
(continued)

| | <u>Page</u> |
|---|-------------|
| <u>APPENDIX B</u> | |
| Detective Quantum Efficiency of Photographic Films | 103 |
| Addresses of Film Suppliers..... | 109 |
| REFERENCES | 110 |

FIGURES

| <u>Figure No.</u> | | <u>Page</u> |
|-------------------|--|-------------|
| 1 | Comparison of Film Noise Power Spectra for the Three Films Tested | 5 |
| 2 | Film Exposure and Measurement Apparatus | 20 |
| 3 | Optical System Noise Spectrum | 26 |
| 4 | Film Noise Versus Amplitude Transmittance Fixed Spatial Frequency | 30 |
| 5 | Amplitude Transmittance Versus Exposure for Photo Horizon's Free Radical Film | 32 |
| 6 | Amplitude Transmittance Versus Exposure for 3M's Dry Silver Film | 33 |
| 7 | Amplitude Transmittance Versus Exposure Curves for Kodak's SO-243 Film, for Wet and BIMAT Processing | 35 |
| 8 | Amplitude Transmittance Versus Exposure for Kodak's 649-F Film, Both Wet and BIMAT Processed | 36 |
| 9 | Film Noise Spectra for Photo Horizon's Free Radical Film | 38 |
| 10 | Film Noise Spectra for 3 M's Dry Silver Film | 39 |
| 11 | Film Noise Spectra for Kodak's SO-243 Film Processed with a BIMAT Film | 40 |
| 12 | Film Noise Spectra for Kodak's SO-243 Film Processed 4 Minutes in D-19 at 70°F | 41 |
| 13 | Film Noise Spectra for Kodak's 649-F Processed with BIMAT Film | 43 |
| 14 | Film Noise Spectra for Kodak's 649-F Processed 4 Minutes in D-19 at 70°F | 44 |
| 15 | Comparison of Film Noise Spectra from BIMAT and Wet Processed Films | 45 |

FIGURES
(continued)

| <u>Figure No.</u> | | <u>Page</u> |
|-------------------|---|-------------|
| 16 | Smearred Star Image Pulses and Their Cross Correlations | 91 |
| 17 | Autocorrelations of Smearred Pulses | 93 |
| B-1 | DQE as a Function of the Log Exposure | 108 |

TABLES

| <u>Table No.</u> | | <u>Page</u> |
|------------------|--|-------------|
| 1 | Characteristics of Several Rapidly Developed Films | 3 |
| | Footnotes - Table 1 | 4 |
| 2 | Table of Currently Available Image Intensifier Characteristics | 10 |
| 3 | Exposures and Exposure Times for the 4th Magnitude Stars | 88 |

1.0 INTRODUCTION

The primary purpose of this investigation is to evaluate various methods of producing photographic records of star field images. These photographic records must be processed rapidly in a spacecraft environment. They must be suitable for use in a coherent optical cross correlator, so that the star fields can be automatically compared with stored reference star maps. While directed toward the star correlator application, the results of this film study are also needed to evaluate the performance of many other coherent optical data processing systems, such as radar processors, spectrum analyzers, and image enhancement systems. The data reported herein may also be useful for conventional incoherent optical imaging systems which might benefit from the use of rapidly developed films.

We have investigated three types of input films, as reported in detail in Section 3.0;

1. Optically developed "Free Radical" films,
2. Heat developed "Dry Silver" films, and
3. Diffusion transfer processed silver halide films.

Since the first two films are relatively insensitive, we have also evaluated the currently available image intensifier tubes which might be used to amplify the weak star images. Section 4.0 describes the performance characteristics of the unclassified image intensifier tubes.

Since the immediate purpose of this study is to provide data pertinent to the design of a star correlator, we have also analyzed the effects of spacecraft motion on the star correlator as reported in Section 6.0. The results of the entire study are summarized in Section 2.0.

2.0 SUMMARY OF INVESTIGATIONS

2.1 Summary Comparison of Film Characteristics

The results of our study of three rapidly developed films are summarized in Table I. The sensitivity, noise, modulation efficiency and exposure range data were all obtained from our measurement program described in Section 3.0. All other information was obtained from manufacturers' specifications or published literature.

Sensitivity - If we use the BIMAT processed SO-243 film as a sensitivity standard, then the Dry Silver film is over 1300 times less sensitive and the Free Radical film is over 24,000 times less sensitive. By comparison, BIMAT processed 649-F, one of the slowest and highest resolution silver halide films, is 400 times less sensitive than SO-243.

Resolution - The resolution of all three films is more than adequate for most optical data processing requirements. Only the SO-243 film with 50% contrast at 100 μ /mm might be marginal for some very high resolution system.

Noise - The complete film noise spectra for the three films are shown in Figure 1. Each spectrum was measured from a test film uniformly exposed to an amplitude transmittance of approximately 50%. The spectrum of 649F high resolution film processed conventionally in D-19 for four minutes is also shown for comparison. The noise data in Table I was taken at the 100 line per millimeter spatial frequency. Again taking BIMAT processed SO-243 as the noise standard, Dry Silver film is seven times noisier while Free Radical film is 3.8 times noisier. No liquid gate was used in these measurements.

Shelf Life - The Free Radical film has limited life time (2 - 3 months) at room temperature, and up to a year under refrigeration. Dry Silver has better storage characteristics, approaching a year even at room temperature. BIMAT film can be stored indefinitely in the dry state, but has limited life once the chemicals have been added to the emulsion.

TABLE I Characteristics of Several Rapidly Developed Films

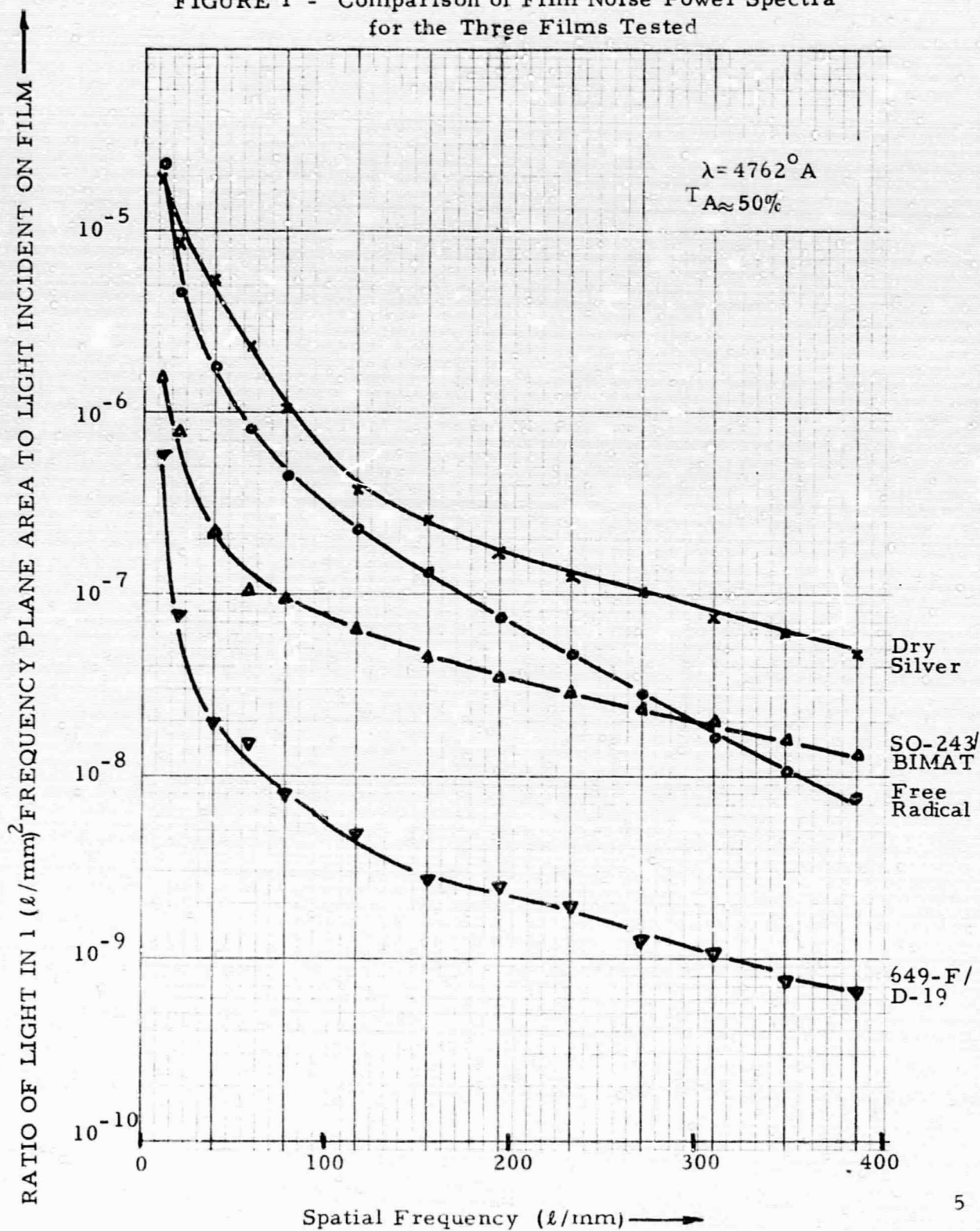
| | Free Radical | Dry Silver | BIMAT | |
|--|---|---|--|--------------------------------------|
| | Type 2000 | Type 7841 | SO 243 | 649F |
| Sensitivity ^a | 3.1×10^{-5} | 5.72×10^{-4} | 0.77 | 1.91×10^{-3} |
| Resolution (50% contrast) | >1000 ℓ /mm | >500 ℓ /mm | 100 ℓ /mm Positive: 10 ℓ /mm ^e | >1000 ℓ /mm |
| Noise Ratio at 100 ℓ /mm ^b | 3×10^{-7} | 5.5×10^{-7} | 7.8×10^{-8} | 8.3×10^{-8} |
| Shelf Life @ 70° F @ 42° F | 2-3 months 9-12 " | 6 to 12 mos. >12 months | 2-3 weeks 3-4 months | >12 months |
| Reciprocity Failure | No failure 10^{-8} to 100 seconds | 10^{-3} sec. 2X 10^{-6} sec. 4X 10^{-7} sec. 8X | 10^{-4} sec-Negl. 10 sec-~2.5X | |
| Modulation Efficiency ^c | .201 | .293 | .159 | .760 |
| Quasi-Linear Exposure Range ^d (ergs/cm ²) | 15,000 to 50,000 | 1,000 to 2,500 | .5 to 2.2 | 300 to 750 |
| Relief Image | $\approx 1\mu$ /N. D. | ? | yes | $\approx .18\mu$ /N. D. ^g |
| Base Thickness | 3-5 mil | 3 mil | 5.25 mil | 5.5 mil |
| Base Material | Polyester | Polyester | Graybase Triacetate | Clear Triacetate (rem jet backing) |
| Latent Image Decay | None after 2 weeks | 20% after 16 days | ? | 57% after 16 hours |
| Development Technique | Optical | Heating to 270°F | Lamination & Diffusion Transfer | |
| Development Time | 10-400 Seconds | 5-20 Seconds | 90 Seconds to 20 Minutes | 90 Seconds to 20 Minutes |
| Fixing Technique | Heating to 140°C for 90 seconds | (One Step) | (One Step) | (One Step) |
| Manufacturer | Photo-Horizons | 3M | Eastman Kodak, Mark Systems | Eastman Kodak |

TABLE I

Footnotes

- a. Sensitivity is defined as the reciprocal of the exposure in ergs/cm^2 required to produce an amplitude transmission in the middle of the linear part of the T_A -E curve. $(1/E)$
- b. The noise figure given is the ratio of the light at 4762 \AA diffracted by a film of about 50% amplitude transmission into a $1 (\lambda/\text{mm}^2)$ area of the transform plane centered at 100 lines per millimeter, to the light incident on the film.
- c. The modulation efficiency is the ratio of the light amplitude percentage modulation for light passing through a sine wave exposed film, (which is equal to ΔT_A) to the percentage modulation of the exposure necessary to produce that sine wave density pattern on film. $\left[\frac{\Delta T_A E}{100 \Delta E} \right]$
- d. The "quasi-linear exposure range" is the exposure range in ergs/cm^2 which produces a film transmittance in the quasi-linear part of the T_A -E curve of the film.
- e. Based on measurement reported in Reference 2 using BIMAT and Plus-X film.
- f. Depth of free radical relief image after development is approximately equal to the density of the local area in density units according to Ref. 3 (e.g., an area of density 1.0 will be about 1 micron thinner than any surrounding unexposed areas.)
- g. Relief image of 649-F based on Figure 17 of Ref. 4, which shows a maximum of 0.6 fringe or 0.18 micron relief image; this film was processed in D-19, however, and BIMAT processing may produce a different relief image.
- h. The latent image decay of 649-GH is reported in Reference 5, Figure 16, as a decrease in density from 2.1 for immediate processing after exposure to a density of 1.2 for a 16 hour delay between exposure and processing, or a 57% decrease in density.

FIGURE 1 - Comparison of Film Noise Power Spectra for the Three Films Tested



Even under refrigeration, the presoaked BIMAT should be used in three to four months.

Reciprocity Failure - The silver halide films have an optimum exposure time; longer or shorter times result in lower densities for a given exposure. The exposure of wet processed SO-243 must be increased about 2.5 times at a 10 second exposure time compared to a one millisecond time.¹ Free Radical supposedly has no reciprocity failure. Dry Silver film has significant high intensity reciprocity failure. A ten megahertz laser recorder would suffer an 8 times loss in sensitivity, for example, and Free Radical film would be only two times less sensitive than Dry Silver for this application.

Modulation Efficiency - An important parameter for many recording systems is the modulation efficiency, or the ratio of the percentage output light amplitude modulation, ΔT_A , resulting from a given percentage change in the input exposure modulation $\frac{\Delta E}{E} \times 100$. A modulation efficiency of 0.5 implies that the exposure must be modulated by 2% to yield a 1% change in amplitude transmittance of the film after development. From Table I, 649F has the highest modulation efficiency, due primarily to its high contrast or large slope of its T_A - E curve. Note, however, that the modulation efficiency is proportional to the product of the T_A - E curve slope and the average exposure level, E. Thus a more sensitive film (lower "E"), would require a steeper T_A - E curve just to maintain the modulation efficiency of 649F. Thus, BIMAT processed SO-243 has a lower modulation efficiency (.159) than 649F (.76), while Free Radical (.201) and Dry Silver (.293) are intermediate, despite their very large required average exposure levels.

2.2 Summary of Image Intensification Investigation

Electronic image intensification is most typically used in situations where the available light level is sufficiently low that long integration times would be required to record the necessary information. In general, intensifiers are avoided if possible because they represent an artificial noise source in the recording loop and constrain the system resolution performance characteristics. In a system application where standard chemical film developing techniques are not practical, the characteristic high luminous gain of these devices (10^4) makes consideration of "pseudo-real-time" recording films possible. As the Film Study Section points out, films such as the dry silver, free radical and BIMAT processed SO243 have characteristic slow recording speeds; thus for short exposure time the incident light flux must be high to obtain suitable recording in the linear region of the T_A -E curve. A point that should be emphasized, is that, if the total system considerations indicate the necessity of electronic image intensification, films intermediate to Royal Pan X and SO243 should be evaluated, because the limiting resolution is determined by the intensifier, and the ultimate system sensitivity at a particular exposure time is determined by the combination of film speed and intensifier gain. Thus, films such as Tri X or Plus X should be evaluated using BIMAT processing techniques for application as direct image recording materials.

In describing image intensifiers, the specific operational parameters and characteristics of image intensifiers are discussed in detail. Equations are developed which describe the resolution, gain efficiency, and noise limiting factors for various interstage coupling arrangements and photocathode-phosphor combinations for two stage image intensifiers. It is shown that the maximum gain, resolution and efficiency is obtained using a fiber-optic interstage coupler and fiber-optic coupled output window for direct film recording applications. The choice of input photocathode depends on the spectral region of interest for detection and the phosphor choice is determined by the recording

film's spectral response. In general, for star fields an S-20 photocathode provides the maximum sensitivity and quantum efficiency. For this application, a P-11 phosphor provides the optimum coupling for both inter-stage and output coupling since its output spectral distribution matches the S-20 photocathode and most recording films. The system configuration which provides the optimum recording capability resembles a framed CRT film recording station in which the recording film is in direct contact with the fiber-optic out window coupler. This technique, as described in detail in the following sections, maximizes the various operational parameters of the electronic-film image intensification system.

In addition to the standard electronic image intensifier systems, a direct electron beam image recording camera "Lallamand Camera", continuous channel plate intensifiers and a novel xerographic intensification system are discussed. The characteristic operational parameters of these intensification systems are discussed only generally due to a lack of extensive information on these systems. The xerographic concept has three very attractive features uncommon to most of the other systems described, they are; (1) the recording resolution is determined by the electron optics resolution (2) no chemical development is necessary and (3) the recording material is inexpensive and not subject to accidental exposure. This system has great potential as a high resolution, real time, nonchemical image recording device but is in the embryonic stage and requires more detailed investigation for systems application.

In the last section of the intensifier report a detailed example is presented in which the image intensifier characteristics are determined by matching its output characteristic to a particular recording film. The criteria for selecting the particular recording film are based on R. C. Jones³⁵ detective quantum efficiency. This really amounts to matching the intensifier's characteristics to the noise characteristics of the film.

This example is calculated for a particular system configuration, as described, using a 0.010 second exposure time, suggested as typical stable time for a space platform environment. Using the available data on various films for detective quantum efficiencies, Royal Pan X film was selected for this example. Using a film output signal to noise ratio of five the ultimate system sensitivity derived was 1.1×10^{-15} watts/cm². This corresponds to a star of the 6th magnitude for an exposure time of 0.010 seconds, an optical aperture of 110 cm², and an intensifier gain of 1113. The general aspects of this calculation can be applied to any of the real time films discussed in the film study section. Obviously, any increase in the exposure time will allow higher ultimate sensitivities in terms of detecting fainter stars. Any increase in exposure time should, however, be coupled with an appropriate change in the intensifier gain consistent with the noise characteristic of the film.

For example, if we use the BIMAT processed SO243 film and constrain the exposure region to the central portion of the T_A-E curve, we find by comparison that using the same system as described in the detailed example, the ultimate sensitivity is approximately 10^{-13} watts/cm². This assumes that the film noise characteristics for SO243 scale approximately as the four reported films of Jones' original article³⁵. It is important to observe that the values derived by Jones are based on RMS granularity measurements. This type of measurement is almost certainly not a good measure of film noise as described in the film noise measurements of this report. It would appear that a more detailed and realistic model is required for application of the detective quantum efficiency concept.

The characteristics of several image intensifiers and the only available channel plate intensifier are summarized in Table II. This table is for illustrative purposes only. These particular tubes have been selected from various manufacturers to give a representative cross-section of currently available devices. The parameters listed are gain, resolution, type

| Manufacturer | Size (Dia.) | No of Stages | Gain | Resolution | Coupler (IC) | Coupler (OC) | N. E. P. | Focussing |
|---|-------------|----------------------|------------------|------------|--------------|--------------|----------------------------------|---------------|
| Aerojet OWLS | 25mm | 1 | 6 | 120 lp/mm | | window | 10^{-11} lum/cm ² | Electrostatic |
| RCA C70021AAP1 | 38mm | 3 | 10^5 | 23 lp/mm | fiber | window | 10^{-14} watts/cm ² | Magnetic |
| ITT F-4706 | 23mm | 3 | 3×10^4 | 17 lp/mm | fiber | fiber | 10^{-11} lum/cm ² | Electrostatic |
| Westinghouse DV1-200 | 38mm | 2 | 3×10^3 | 36 lp/mm | fiber | window | 10^{-13} watts/cm ² | Magnetic |
| RCA C70056 | 38mm | 2 | 1×10^3 | 18 lp/mm | mica | window | 10^{-13} watts/cm ² | Magnetic |
| RCA C70055 | 87mm | 3 | 2×10^4 | 17 lp/mm | mica | window | 10^{-13} watts/cm ² | Magnetic |
| ITT F-4051 | 25mm | 1 | 50 150 | 45 lp/mm | input fiber | fiber | 10^{-11} lum/cm ² | Electrostatic |
| Channel plate Mullard Res. Laboratories 40G-40S | 40mm | 40μ channel diameter | 10^3 10^7 | 10 lp/mm | - | window | - | Electrostatic |

Table II - Table of Currently Available Image Intensifier Characteristics

of interstage coupler (IC), number of stages noise equivalent power (NEP), output coupler (O.C), focussing method and size. The resolution quoted is derived from a modulation transfer curve at the 10 per cent contrast level for paraxial resolution. Higher resolution, lower noise, total fiber optic coupled intensifier tubes, are available but are classified.

Finally, the intensifier parameter calculations and system example contain the necessary detailed information for suitable parameterization to be applicable to system changes such as, gain recording film or optical configuration.

2.3 Summary of Star Image Smearing Study

We have analytically investigated the effects of star image motion on the correlation process. The preliminary conclusions are that

1) The reference star map should be smeared prior to the generation of the matched filter for optimum sensitivity and correlation signal to noise ratio, but this approach is impractical because a separate Vander Lugt filter is required for each angle of motion within each field of view in space.

2) Given the matched holographic filter of an unsmeared map, the correlation signal to noise ratio does increase linearly with smear length if an appropriate "line integrating" light detector is utilized, and

3) Even the more sensitive SO-243 BIMAT processed film requires an image intensifier and an image smeared by 13 star diameters to detect 4th magnitude stars at a 4 rpm spin rate.

These conclusions should be verified experimentally.

3.0 DETAILED DESCRIPTION OF FILM INVESTIGATIONS

A photosensitive film, to be useful in a coherent optical system must have adequate sensitivity and resolution. It must not have severe reciprocity failure at the required exposure times, and the film must have adequate shelf-life for the application. This information can normally be obtained from the manufacturer. Two other film characteristics (noise and input-output transfer curve) are not readily available in a suitable form. For example, the complex grain noise characteristics of conventional silver halide films are typically represented by one number, the "RMS granularity." In reality, the noise power in a photographic film varies with spatial frequency, with development conditions, and even varies significantly with the recorded signal or the average density level. One averaged number certainly cannot represent this complex noise source. In this investigation we have therefore measured the complex noise characteristics of the various films. The noise data is reported in terms of the power spectrum (ratio of light diffracted into each spatial frequency interval to the light incident on the film) for different uniformly exposed pieces of film.

Another set of measurements were made to determine the films' transfer characteristics. This data is usually reported by the manufacturers of silver halide films in terms of the Hurter & Driffield (H & D) curve. This is a plot of the density of the developed film versus the logarithm of the exposure. Coherent optical systems are generally analyzed in terms of the light amplitude in the system, since a Fourier transform relationship exists between the light amplitude distributions in the back and front focal planes of a lens. The appropriate output characteristic of a film is therefore its amplitude transmittance, T_A . The amplitude transmittance is in general a complex quantity, accounting for both intensity fluctuations and light phase variations caused by the film. If the phase variation were insignificant (this is not normally true), then " T_A " would be the square root

of the intensity transmittance, T_I , and since the film's density is given by

$$D = -\log T_I,$$

the density and amplitude transmittance are related by

$$D = -2 \log T_A.$$

Taking the logarithm of either the input (Exposure, E) or the output (T_A) does nothing but obscure the important characteristics of the film for a coherent system.

Linearity is of primary concern in spectrum analyzers, image restoration systems, and, to a lesser degree, in cross correlators. Non-linearities can cause intermodulation distortion, harmonics, and false targets in radar processors. The $T_A - E$ curve should therefore be linear about the operating bias points for these systems. But the linear part of the $T_A - E$ curve corresponds to the "toe" of the H & D curve. We therefore measured $T_A - E$ curves for all the films investigated.

3.1 Description of Unconventional Films Investigated

Three unconventional films were investigated in this program. The basic characteristics of these films are described below, while the transfer curves and noise spectra for each film are presented in Section 3.3.

3.1.1 Free-Radical Film

Free-radical films are photosensitive materials which produce small quantities of organic dye in a chemical reaction instigated by short wavelength light exposure. A novel type of "latent image" is formed in this manner. This weak latent image can then be amplified 100 times or more by uniformly exposing the film to longer wavelength light which the latent image dye absorbs. The initial short wavelength sensitivity is destroyed by heating the film. Thus the film is optically developed and fixed by heating. No chemical processing of any type is required. For a detailed description of the chemistry of this process and a list of other references, see References 6 and 7.

The free radical film used in this investigation was supplied by PhotoHorizons which is a Division of Horizons Research Incorporated of Cleveland, Ohio. This film, Type 2000, is sensitive in the blue region of the spectrum with a peak sensitivity at about 4050°A , with reasonable sensitivity extending out to 5000°A .

The performance of this film appears to be limited by the non-uniformity in the coating of the emulsion on the base. PhotoHorizons is installing a new coating alley which should improve the quality of the coatings. The present coatings have thickness variations which are apparent to the eye. Even minute changes in thickness may ultimately produce variations in developed density after the optical development process.

The manufacturer generously loaned us one of their Model 101 Optical Processors for our tests. This unit includes a 1 kilowatt General Electric tungsten-halogen lamp and a Corning No. 2408 (CS-2-60) glass filter to attenuate the blue light during the development process. A Model 102 motorized cut film transport was also supplied. This transport moves the

film under the lamp. Unfortunately, very small changes in the velocity of this drive produce large changes in the density of the developed film. We had to clean the drive unit to achieve even moderate development uniformity across a 4 inch piece of 35 mm film. Even then thermal gradients generated by the 1 kw lamp made uniform development very difficult. Therefore, Photo Horizons offered to optically develop and fix some test exposure films in their laboratory processor. All of the data presented in Section 3.3 was derived from four test strips processed by Photo Horizons.

It should be noted that even the test films developed in the manufacturer's controlled processor did not have uniform density. This was particularly noticeable at low densities, where a uniformly exposed area appeared "mottled" after development. Presumably the new coating alley will improve this low spatial frequency noise.

Higher sensitivity free radical films are available, but these types generally have a reduced shelf life. For space applications, however, reference 6 notes that the sensitivity increases about 15 times in a vacuum, due to the absence of oxygen.

3.1.2 Dry Silver Film

Dry Silver film, manufactured by 3M, is also a nonchemically developed blue sensitive film. This film is developed and fixed in a single step by the application of dry heat. The film used in this investigation, 3M's Type 7841, is sensitive to wavelengths from UV out to 5500°A , with a peak sensitivity at 5300°A . Another 3M film has been reported⁸ with a peak sensitivity at 6328°A , the helium neon laser red line, but this film is not commercially available. The type 7841 film has a colored antihalation layer which is removed by the heat development process.

The dry silver films used in this study were processed by hanging them inside a Tenney Engineering oven. The recommended development conditions are 15 to 20 seconds at 280°F . Opening the oven door to insert the test films unfortunately lowers the ambient air temperature. The

development conditions are therefore dependent on the time the door is opened, which is difficult to control. To minimize this effect, we lowered the oven temperature to 250^oF and extended the development time to 40 seconds. This procedure yielded reasonably uniform and repeatable film densities.

For optimum uniformity of development, 3M recommends immersion of the films in a liquid fluorochemical, 3M type FC-40. The films can also be developed by contact with a hot platten, but heat transfer irregularities generate density variations. The development time can also be reduced to a few seconds by increasing the development temperature, but the temperature must be more carefully controlled, since minute changes in temperature will have a greater effect on the developed density.

The contrast of the 3M Type 784 films can be varied by changing the development time. Longer development produces higher contrast and higher effective sensitivity, as with silver halide films.

3.1.3 BIMAT Transfer Films

Diffusion transfer films are not photosensitive, but are actually chemically soaked "webs" which are used to develop conventional silver halide negatives. After exposure, the negative film is laminated to the web, usually by a set of pressure rollers. The chemicals from the BIMAT "film" diffuse into the emulsion of the negative and both develop and fix the image as described by Rott⁹. The two films are left in contact for 90 seconds to 20 minutes depending on the negative film emulsion thickness. The films are then separated. The negative can be analyzed immediately, but, for archival quality, should be washed and dried in the usual manner.

Although the process is chemical, there are no free liquids, and the Kodak BIMAT process has been used successfully in space to develop the Lunar Orbiter photographs. (The BIMAT films used in this investigation did not have the same chemistry as the films used in the Lunar Orbiter spacecraft.¹⁰) The earliest web process introduced by the Eastman Kodak Company in 1962 was designed to process Kodak's Special High Definition Aerial Film (Gray Base), Type SO-243¹¹. Later Kodak BIMAT films not only develop the negative film but also produce a lower quality positive image in the BIMAT emulsion. These BIMAT films have since been used to process thicker emul-

sions of the Plus-X variety in addition to the SO-243 high resolution films.¹²

The image quality of the BIMAT processed negative is comparable to the quality of the negative processed by the conventional wet process.¹³ The resolution as indicated by the modulation transfer function (MTF) for Plus-X film is even slightly better with BIMAT processing.¹³ Grain noise is claimed to be similar,¹² although our results reported in Section 3.3 below indicate moderate increases in noise with BIMAT processing.

The major drawback of BIMAT processing for coherent optical systems is the reduced dynamic range as a result of increased fogging of the film.¹⁴ This fog level is reduced by cooling the two films during processing,¹⁰ but time did not permit a complete study of this effect during the existing contract.

The development time for BIMAT processing varies from fifteen minutes for Plus-X to 90 seconds or less for SO-243 films. The development time may be much shorter for very fine resolution films such as Kodak's 649-F, although again, more research is required. One advantage of the diffusion transfer process is that the time of development is not critical. Once the process is completed, increased contact between the films has little effect on their image characteristics.

To use the BIMAT process in our laboratory, we initially used simple hand rollers to laminate the BIMAT film to the negative film. This technique was not successful, since air bubbles produced undeveloped areas in the test films. Good quality films were eventually developed by passing the two films through the rollers of a Kodak Ektamatic photographic paper processor (with the chemicals removed).

The BIMAT films do have a limited storage life once the chemicals have been added to the emulsion. For this reason the BIMAT film is supplied dry and the chemicals are added in a "pre-soaking" operation prior to use. The Eastman Kodak Company will reportedly discontinue supplying the pre-soaked BIMAT films in early 1970.¹⁵ We therefore obtained the type 2436A pre-soaked BIMAT film from Mark Systems of Cupertino, California.

3.2 Description of the Film Measurements Equipment

To evaluate the noise and transfer curve film characteristics pertinent to a coherent optical processor, we had to perform three separate operations. The film was exposed to varying degrees, the amplitude transmission was measured for each exposure level, and the film noise spectra was measured for selected frames. One optical system was designed to perform all three operations as described below.

3.2.1 Exposure Station

The "exposure" of a film is defined as the integral of the light intensity illuminating the film over the time that the light is on, " τ ".

$$E \equiv \int_0^{\tau} I dt$$

If the intensity is constant over the interval, then the exposure reduces to a simple product

$$E = I\tau$$

The exposure station must therefore illuminate the film under test with a known level of light intensity for a known period of time. An auxiliary goal is that the light source be at least quasi-monochromatic so that the effects of different exposing light wavelengths can be explored.

No graduated density step tablets were used in these experiments. These step tablets have some spatial noise, particularly in coherent light. Their noise would certainly add to the noise of the films under test. In place of the step tablets, we exposed each film to a set of different time durations of some constant light irradiance. We have thus ignored reciprocity failure, assuming that the film responds directly to the product of time and light intensity.

3.2.1.1 The Exposing Light Source

A Krypton laser was chosen as the exposure source for this investigation. The advantages of a laser for this exposure application include its narrow collimated beam which facilitates the shuttering operation and the directional control of the light beam, its relatively constant amplitude with time, its intensity, and its monochromaticity. The disadvantages of a laser illumination source would preclude its use, unless the exposure station is carefully designed. These disadvantages stem from the coherence of the laser. Due to its spatial coherence, minute particles of dust or other imperfections in the optics generate noisy diffraction rings in the laser light pattern. This erratic light pattern would not suffice as the constant intensity source. One standard solution is to pass the beam through a short focal length lens which focuses the beam through a small pinhole. The pinhole passes only the "DC" light, blocking the higher spatial frequency noise pattern. This lens also serves to diverge or expand the narrow laser beam so that it can expose a 35mm frame of film. The light is further averaged by reflecting it from a rotating mirror which is cocked at a slight angle, as shown in Figure 2. This rotating mirror also helps to average the Gaussian laser beam spatial pattern.

While the spatial coherence of the laser produces a noisy illumination pattern in space, the temporal coherence creates another type of "exposure noise" when the film is placed in the expanded laser beam. Light reflected from the base of the film travels back toward the source. This light interferes with the incident laser light. The interference is constructive (resulting in a build-up of effective exposure) or destructive (resulting in a reduction of exposure) depending on the thickness of the film. Very small changes in film thickness (on the order of the wavelength of light) therefore produce a set of random interference fringes on the developed film. These fringes can be reduced to a negligible level by carefully choosing the geometry

EQUIPMENT

1. Coherent Radiation Labs Model 52 Krypton Laser
2. Electro-mechanical Shutter
3. Glass beamsplitter
4. Light Detector
5. Microscope Objective Lens, 20X
6. Pinhole, ~25 micron dia.
7. Rotating, tilted mirror (Removed for film measurements.)
8. Aperture Mask
9. Nikon Camera Back (no lens)
10. Spectra/Physics Model Light Meter
11. Amplifier
12. Hewlett Packard Model 6518 Oscillator
13. Systron Donner Model 114 Counter
14. Heath Model PT 15 Timer
15. Schneider-Kreuznach Tele-Xenar 360mm Lens
16. Film Under Test (1-3/32" x 29/32")
17. Spectrum Scanner
18. 1.5 mm Dia. "Pinhole"
19. Diffusing Screen
20. RCA 1P21 Photomultiplier
21. FET Operational Amplifier
22. Tryptics Series 4000 Digital Voltmeter

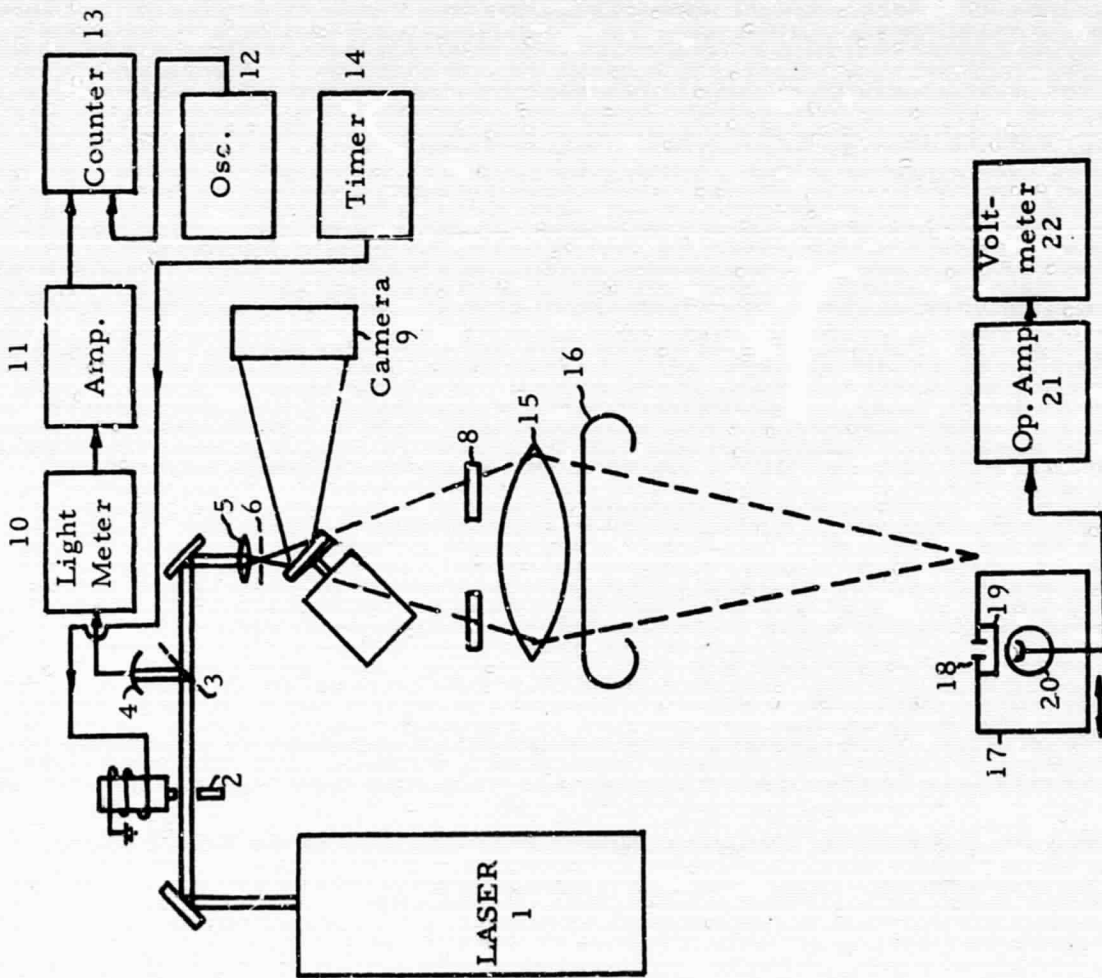


Figure 2 - Film Exposure and Measurement Apparatus

of the film plane relative to the laser beam, taking advantage of the fact that for parallel polarized light, the reflection from a denser medium (film) to a rarer medium (air) is reduced if the angle of incidence is increased. Indeed, for a lossless medium, there is a principal angle for parallel polarized light where there is no internal reflection.¹⁷ At a slightly larger angle, however, the critical angle is reached where there is total internal reflection for the ideal lossless medium. For practical film bases, the angle of incidence can be rather large with a significant decrease in the observed interference fringes. An incidence angle of 50° was arbitrarily chosen for all exposures in this study.

The intensity of the laser was measured at the film plane with a standard Spectra/Physics Model light meter. Simultaneous measurements were also made via a beam splitter at a monitoring station as shown in Figure 2. The meter power reading at this monitoring station was then calibrated in terms of the light irradiance at the film plane in watts per square centimeter (watts/cm^2). This calibration required a measurement of the light probe effective area, the spectral response of the power meter*, and included a cosine law correction for the projected area of the 50° tilted film plane. By this technique, the light irradiance could be monitored remotely to an estimated accuracy of 15% for any exposure. Most of the error in the irradiance estimation is in the power meter itself, which the manufacturer claims is accurate to 10%. The relative intensity accuracy between any two exposures of this test is estimated at 5%.

*The meter is calibrated for the 6328° red laser line, while all measurements reported herein were made at 4672° A.

3.2.1.2 The Exposure Timing System

The exposure timing system used in this program combines a relatively crude electromechanical shutter and an accurate time measurement system. Thus the preset exposure time may not be achieved with any accuracy better than 20%, but the actual exposure time is monitored and recorded for every exposure to an accuracy of two milliseconds. This corresponds to a 2% accuracy for the shortest exposure times used (100 milliseconds), and a proportionately higher accuracy for longer exposure times.

The timing system is diagrammed in Figure 2. The shutter is simply a modified relay coil with the relay contacts replaced by a thin shutter blade which interrupts the narrow laser beam. The shutter is actuated by a Heathkit Model PT 15 laboratory timer. This timer is not highly accurate, and the relay coil opening and closing times varies 10 or 20 milliseconds from one exposure to the next.

The exposure time cannot be set accurately before the film frame is exposed. Once the shutter has opened, however, the monitoring system clocks the exact exposure time to better than 2 millisecond accuracy. As shown in Figure 2, this timing system uses the Spectra/Physics power meter to sense when the shutter is open. The light detector output is amplified and then triggers a counter. The counter is driven by an oscillator, which is set at a one kilocycle frequency. Each count therefore represents one millisecond of actual laser beam "ON" time.

3.2.3 The T_A - E Curves

The amplitude transmittance (T_A) versus exposure (E) curves were produced by exposing a set of 35 mm frames to varying time durations of some uniform laser irradiance. The level of exposure for each frame was determined from the product of the laser irradiance measurements and the exposure time measurements described in Section 3.3.1 above.

The amplitude transmittance of the developed film was measured in the coherent optical system of Figure 2 (the dashed lines). This system is a basic optical spectrum analyzer. By placing the photomultiplier and pinhole assembly on the optical axis, we measured the "DC" or average light component. The procedure for each frame of a test film was to insert that frame, read and record the photodetected voltage, and then to remove the film and immediately note the "clear aperture" DC voltage. The ratio of these two voltages yields immediately the specular intensity transmittance. The amplitude transmittance is then taken as the square root of this ratio.

Note that we are measuring the specular amplitude transmittance as opposed to the diffuse or even doubly diffuse (or some combination thereof) density normally measured on a densitometer. That is, the film is illuminated with nearly collimated light and the photomultiplier pinhole "sees" only the DC or average light level. Any light which is diffracted into even a very small angle by film noise will not be detected. Therefore, these specular transmittance measurements will normally be lower than diffuse transmittance measurements of the same film. (Diffuse density is less than specular density). This is as it should be, since any light contribution which increases diffuse transmittance over specular transmittance is really film noise, and will be properly measured in the film noise power spectral measurements described below.

3.2.4 Film Noise Spectra

The most useful and informative method of representing film noise is by its power spectrum. The film noise power spectrum is essentially a plot of the amount of light scattered by the noise sources into each angle or into each spatial frequency interval. It is normally plotted as a ratio of the light power diffracted into a one line per millimeter square area divided by the light power incident on the film. Other simplified film noise measures such as "RMS granularity" can be derived from the power spectrum.

The noise power spectrum is measured by inserting the uniformly exposed film frame into the coherent optical system of Figure 2. The light amplitude distribution in the focal plane of the "transform lens" is theoretically the two dimensional Fourier transformation of the noise pattern. The photomultiplier detects the magnitude squared of this transform which is the power spectrum. The spectrum is sampled by physically moving the pinhole-photomultiplier system across the transform plane.

The above description of power spectral measurements is relatively straightforward. In practice, however, there are two major difficulties: Dynamic range and optical system noise. The dynamic range of the power spectrum may be as high as 100 dB for some fine-grained emulsions. Photomultipliers have linear responses over ranges approaching 70 to 80 dB, but the subsequent electronics have a reasonably linear dynamic range of only 30 dB. To overcome this practical difficulty, we inserted neutral density filters into the laser beam to attenuate the relatively bright lower frequency spectral data and thereby cut down the dynamic range. These neutral density filters were calibrated by the same technique used to measure the specular amplitude transmission of the test films. Since these filters are inserted before the spatial filtering pinhole, they do not add noise to the measured power spectra.

The second practical difficulty, optical system noise, is more difficult to handle. Any lens contributes significant noise to a coherent optical system. Dust, glass nonhomogenities, glass surface imperfections, etc., all contribute some noise¹⁷. Figure 3 compares the diffraction limited light level for a diagonally oriented square aperture versus the light level actually measured for the system of Figure 2 with no input film. The single lens between the input spatial filtering pinhole and the output transform plane contributes about 80% of this extra light. (Approximately 10% is due to light scattered from dust particles in the air and 5% is due to other stray light.) This lens used in these measurements was selected for its low noise qualities. In general, the lowest noise lenses have the fewest elements, indicating that glass surface roughness is the prime contributor to lens noise.

Ideally, we would like to separate the film noise from the system or lens noise. To approximate this separation, we measured the "clear aperture" or system noise spectrum without any film, and then measured the spectrum with the film in place. Note that the film actually attenuates the system noise, but also generates more noise of its own. We have assumed, therefore, that the measured power spectrum with the film in the system, $V_m(u)$ is equal to the sum of two noise sources:

$$V_m(u) = V_f(u) + T_I V_s(u) \quad (1)$$

where $V_m(u)$ = the power spectrum with the film in the system

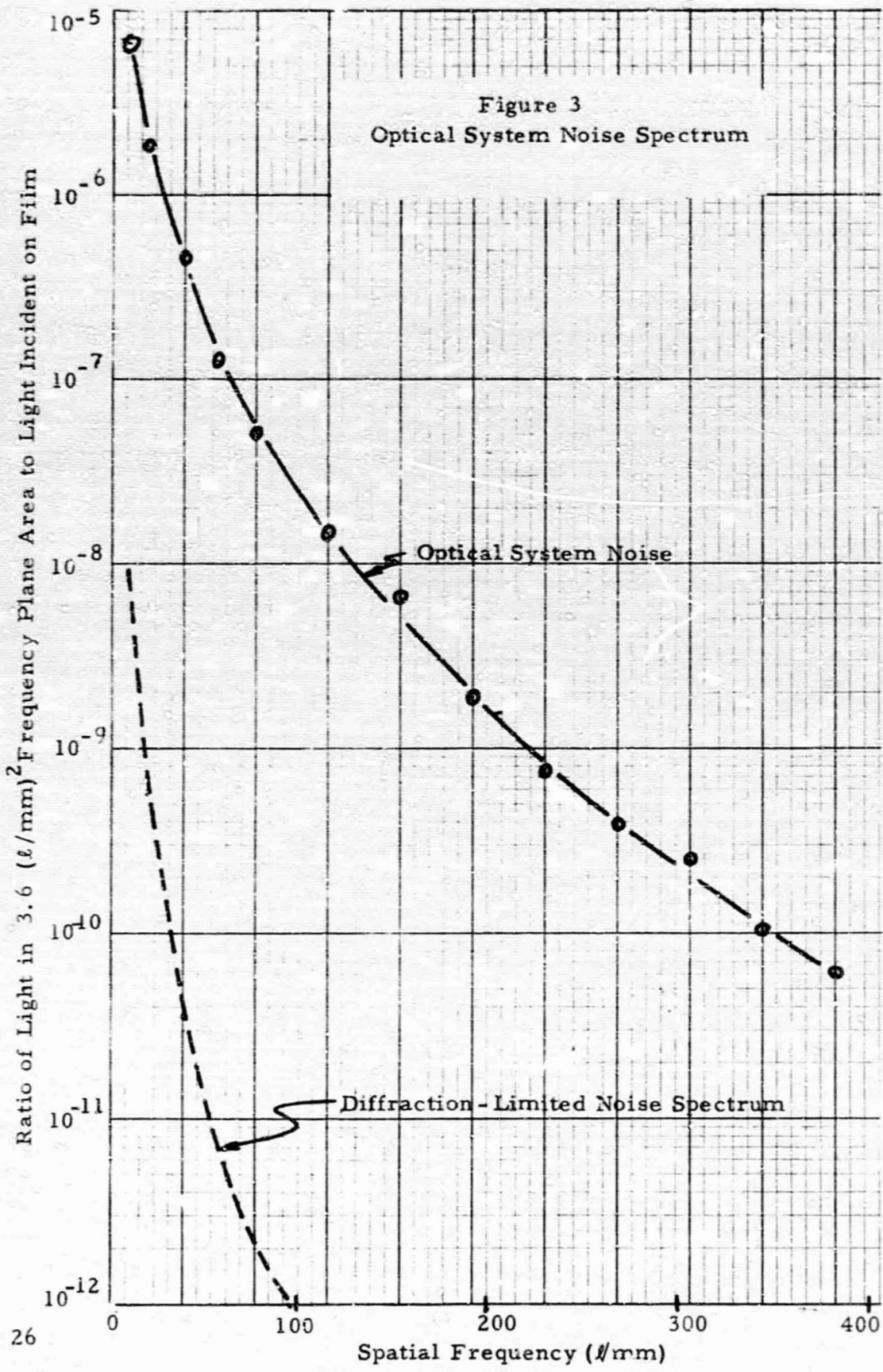
$V_f(u)$ = the power spectrum of the film noise alone.

T_I = the specular intensity transmittance of the film

$V_s(u)$ = the power spectrum of the system alone

u = the spatial frequency plane space dimension*

*We have assumed a rotationally symmetrical two dimensional power spectrum unless otherwise noted; the spectra can therefore be represented as functions of one variable.



Data manipulation is therefore required to extract an estimation of the film spectrum $V_f(u)$, from the three measured quantities:

$$V_f(u) = V_m(u) - T_I V_s(u). \quad (2)$$

There are at least two assumptions explicit in Equation 2.

First we have assumed that the two noise powers add directly. Then we have assumed that the average transmittance, T_I , acts uniformly on all spatial frequencies of $V_s(u)$. While these assumptions may be questionable, the results of this data manipulation should be adequate for comparing the noise characteristics of various films.

The actual spectral data is collected by recording the photoelectric voltage generated by the diffracted light in the transform plane passing through a small aperture. This aperture should be sufficiently large to average local spectrum variations, but small enough to record the gross variations in the film noise power spectrum. Eventually the data is normalized to an aperture with an area equal to one line per millimeter squared. For these experiments the actual aperture had an area corresponding to $3.6 \left(\ell/\text{mm} \right)^2$.

The data is also normalized by the DC or average light level with the film removed from the system. This level represents the light incident on the film. Some researchers have normalized their data by the DC light level with the film being measured left in the system. This procedure yields the ratio of diffracted light to the average transmitted light (instead of the incident light). This makes high density (low transmission) films appear more noisy. This approach may stem from a desire to make the spectral noise data comparable to other photometric measures such as RMS granularity which does increase with increasing density.

Experimental data showing the variation of film noise with amplitude transmission is plotted in Figure 4, for a fixed spatial frequency. Similar curves are obtained at other spatial frequencies. At high transmittances, phase noise predominates, and the noise with no exposure is due almost entirely to phase perturbations. If a liquid gate were used to remove the film thickness variations, this high transmittance noise would decrease significantly, and the noise versus transmittance plot would assume a more nearly symmetrical shape, approaching zero at $T_A = 0$ and $T_A = 100\%$.

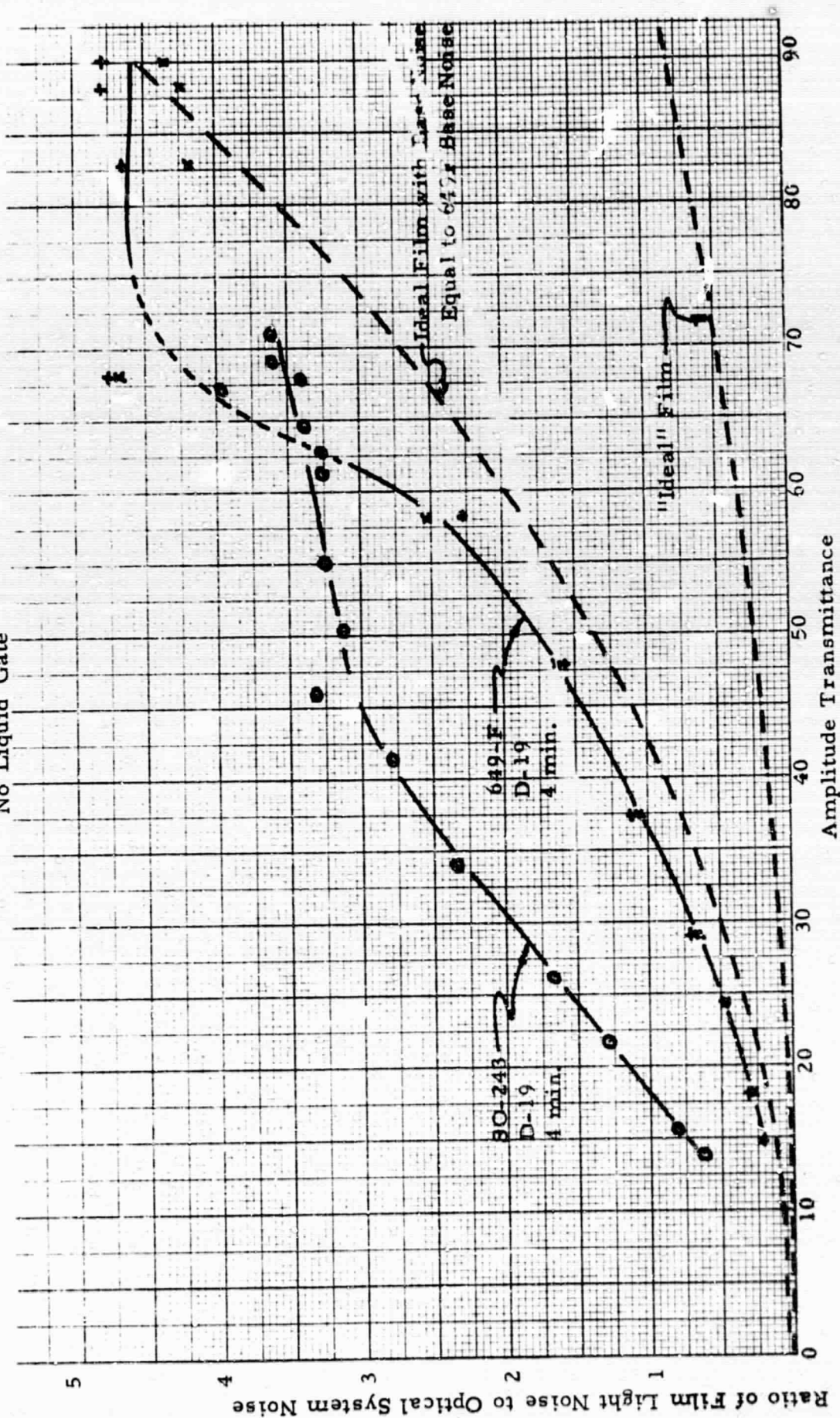
The data for Figure 4 was obtained by recording the photoelectric voltage with a film frame in the system, V_m , and immediately removing the film and noting the "clear aperture" or optical system noise voltage, V_s . The abscissa of Figure 4 is the ratio of (V_m/V_s) . Note that for transmittances below 36% for 649F film, there is less noise voltage with the film in the system ($V_m/V_s < 1$) than with the film out of the system. Thus the film attenuates the optical system noise more than the noise level that it adds.

At high transmittance, phase noise obviously predominates, with the unexposed base of 649F film scattering 4.5 times more light into the 116 ℓ/m region than the optical system itself. This phase noise probably does not depend on the exposure level, except to the extent that increased film density attenuates this phase noise. The upper dashed curve of Figure 4 is a plot of V_m/V_s for a hypothetical "ideal" film which has no grain amplitude noise, but has the same phase noise as 649F. In a sense the deviation of the measured data from this line is an indication of the film's amplitude or grain noise. The difference noise level between this upper dashed curve and the SO-243 noise curve has a peaked character in the region of $T_A = 45\%$. The 649F curve has an unusual deviation in the region near $T_A = 70\%$ which should be investigated further. The lower dashed curve of Figure 4 is for an "ideal" grainless film with no phase noise; this ideal film merely attenuates the optical system noise as its transmittance decreases. There is an obvious need to repeat these measurements with the film in a liquid gate to reduce at least that part of the

phase noise which is due to random relief patterns or film thickness variations.

A noise measure which increases with density can be justified for evaluating imagery in the following sense: If a photo-interpreter is viewing two negatives with differing average densities, and if he increases the average illumination level from his light table such that both negatives have equal average transmitted light, then indeed the denser negative will appear more grainy. If, on the other hand, there are two local areas on a single negative with different average density, (or if the PI does not or can not adjust his light table intensity) then each area receives the same incident illumination level. If the average amplitude transmittance of both areas is less than about 50% (i. e., average density is greater than 0.6) then the denser area will actually generate less absolute light noise. The ratio of grain noise to transmitted light is higher in the denser region, but the ratio of transmitted light in the dense area to that in the less dense area is smaller yet. Thus the ratio of film generated light noise to the incident light level is often higher for the lower density areas of a film.

Figure 4 Film Noise Versus Amplitude Transmittance
 Fixed Spatial Frequency = 116.4 l/mm
 $\lambda = 4762 \text{ \AA}$
 No Liquid Gate



3.3 Detailed Results of the Measurements Program

Two fundamental properties of the films were measured during this program: Transmission versus exposure (T_A -E) curves and film noise spectra.

3.3.1 Amplitude Transmission versus Exposure Curves

The Krypton laser apparatus used to expose the films is described in detail in Section 3.2.1, while the techniques used to measure amplitude transmission is described in Section 3.2.2.

3.3.1.1 Free Radical T_A -E Curve

The T_A -E curve for the free radical film is shown in Figure 5. This data was derived from four separate pieces of film which were exposed by KMS, developed by Photo Horizons in their controlled processor, and finally analyzed by KMS. Each symbol on Figure 5 represents data taken from a different film. The low density frames (greater than 50% amplitude transmission) were quite mottled, accounting for some of the scattered data points above 50% transmission. The linear exposure range appears to be in the range from 15,000 to 50,000 ergs/cm^2 at 4762 $^{\circ}$ A, although the curve is not significantly non-linear for larger exposures and more uniform coating techniques may extend the useful range to lower exposures by reducing the low density mottled effects.

3.3.1.2 Dry Silver T_A -E Curve

The T_A -E curve for four dry silver test films is plotted in Figure 6. Again four films were exposed and individually processed by inserting them in a Tenney temperature controlled oven for 40 seconds at 250 $^{\circ}$ F. The spread of data points may be entirely due to a variation in the development conditions. Based on this data, the useful linear exposure range extends from 1000 to 2500 ergs/cm^2 , although the entire curve appears to be concave upward above 1000 ergs/cm^2 .

Figure 5 - Amplitude Transmittance Versus Exposure for Photo Horizon's Free Radical Film ($\lambda = 4762 \text{ \AA}$)

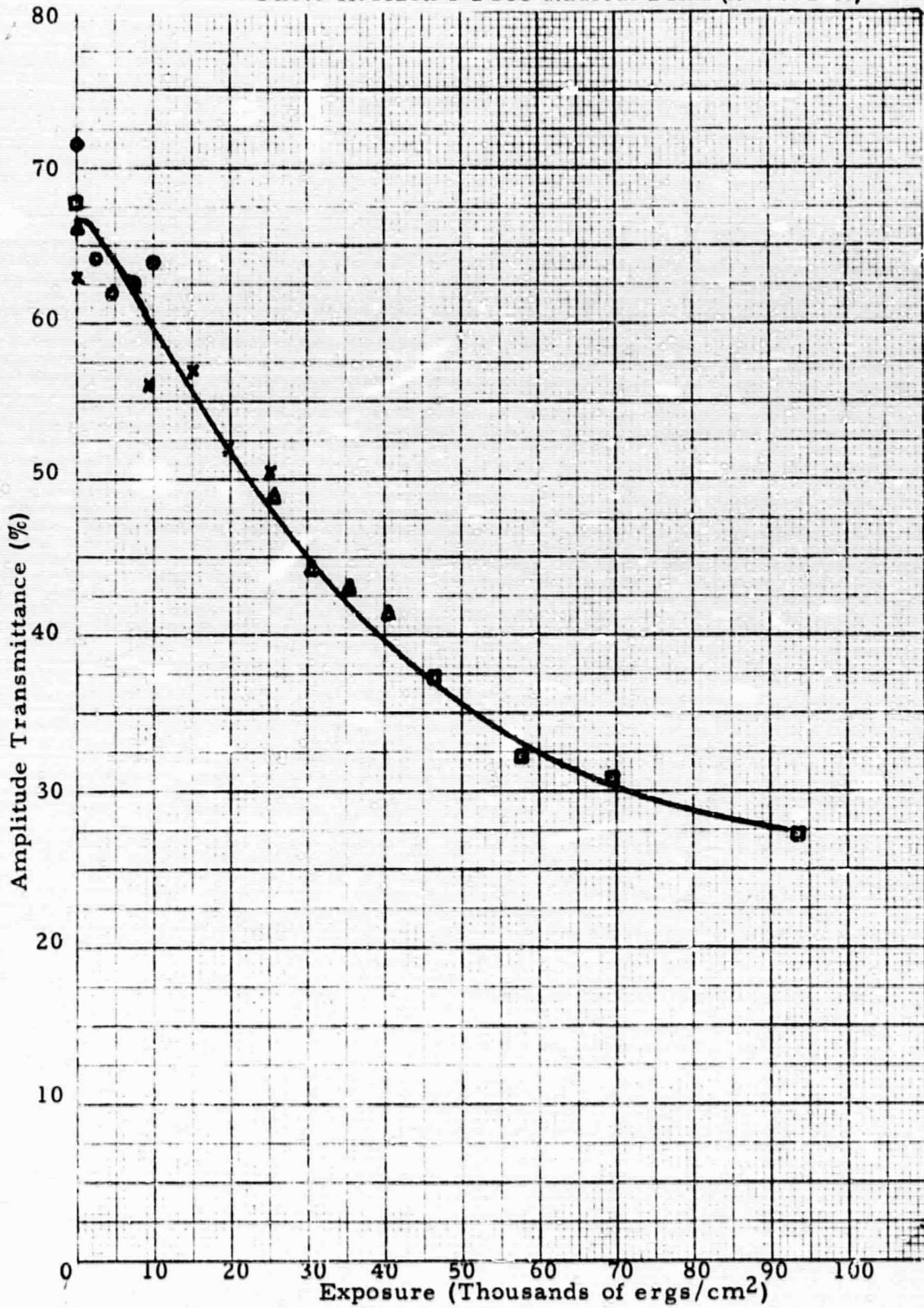
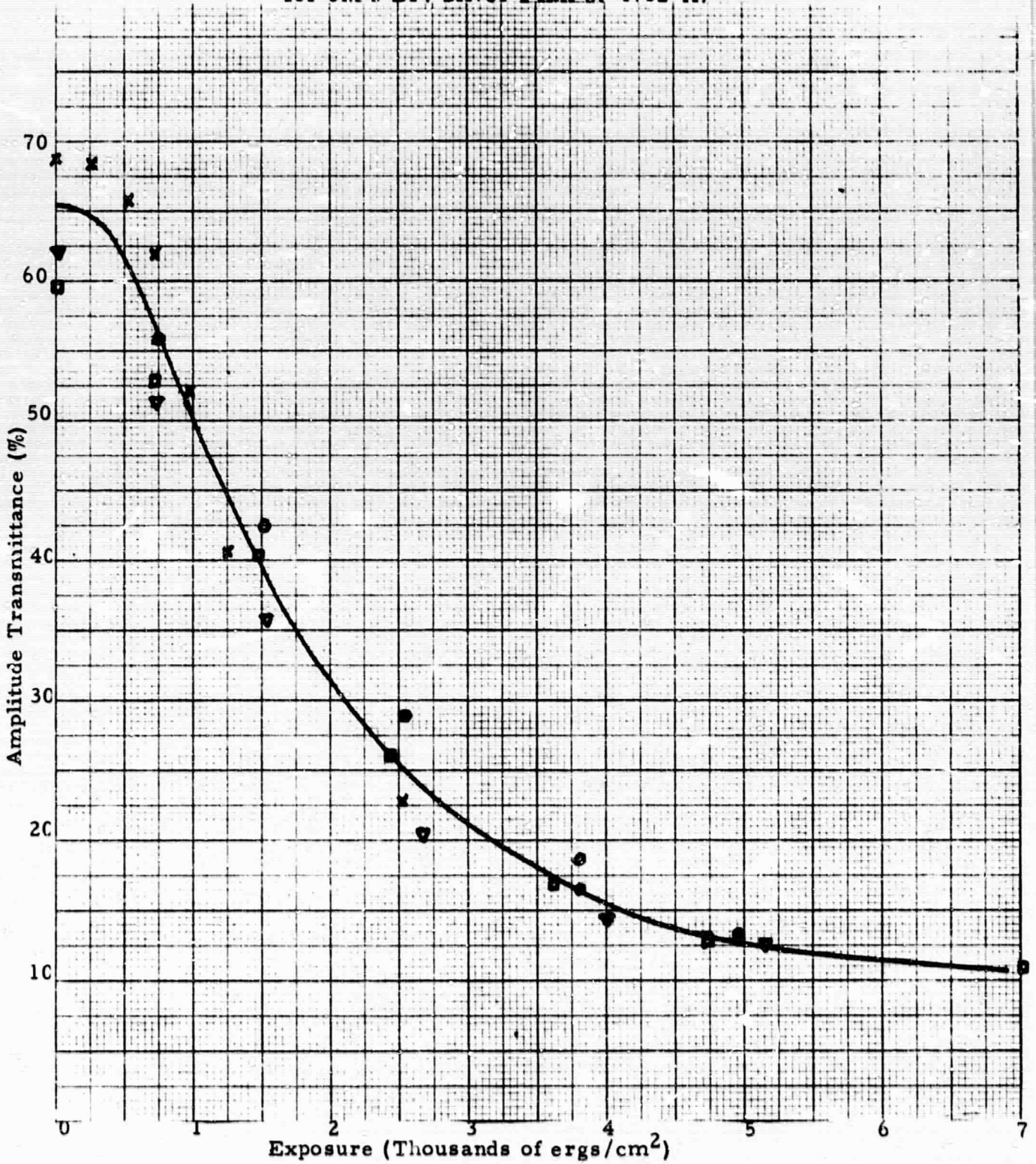


Figure 6 - Amplitude Transmittance versus Exposure
for 3M's Dry Silver Film ($\lambda=4762^{\circ}\text{A}$)



3.3.1.3 BIMAT Processed T_A -E Curves

The Eastman Kodak type 2436A BIMAT film was used to develop both SO-243 and 649F films. The T_A -E curves for SO-243, processed conventionally in D-19 for four minutes at 70°F and processed with the BIMAT film for five minutes, are plotted in Figure 7. (Note: The T_A -E curve does not change significantly for processing time in excess of about 1.5 minutes.) The average speed is not significantly changed by BIMAT processing, but the fog level is increased (as indicated by the lower transmission with no exposure), the contrast (slope) is reduced, and the maximum density (minimum transmission) is reduced slightly. The input quasi-linear exposure range is approximately equal for both processes, extending from about 0.5 to 2.2 ergs/cm². The diffraction efficiency or light modulation of the conventionally processed film will be higher, however, due to the higher contrast. This would increase the signal to system noise ratio in a coherent optical processing system for the wet processed film relative to the BIMAT processed film.

The same comparison of wet processing and BIMAT processing is shown in Figure 8 for the 649F negative emulsion. The 649F films were held in contact with the BIMAT film for three minutes. The minimum processing time is not known for 649F, but it should be less than 1.5 minutes. Again the fog level is increased with BIMAT processing, but the effective sensitivity is also increased relative to processing four minutes in D-19, since it takes less than half the exposure to produce a given transmission. The effect of the BIMAT processing temperature was also briefly investigated. The BIMAT film was placed in a 60°F oven along with the 649F film. They were removed briefly for the lamination process, and then returned to the 60°F environment for three minutes. The fog level was significantly reduced, resulting in an increase in base amplitude transmission from 36.7% for room temperature processing (76°F) to 58% with 60°F processing. This temperature dependence should be pursued further for 649F

Figure 7 - Amplitude Transmittance versus Exposure Curves for Kodak's SO-243 Film, for Wet and BIMAT Processing ($\lambda = 4762^{\circ}\text{A}$)

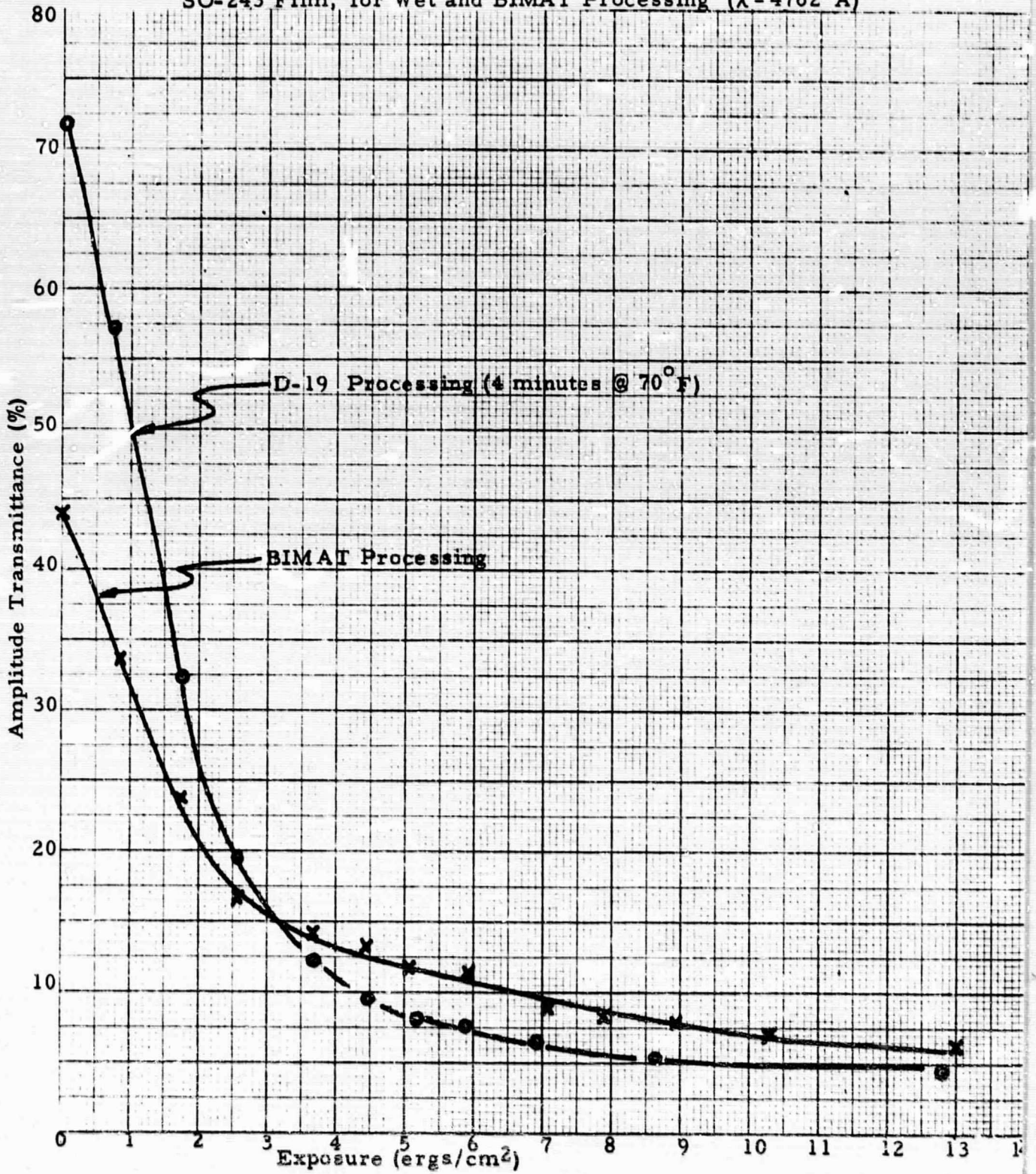
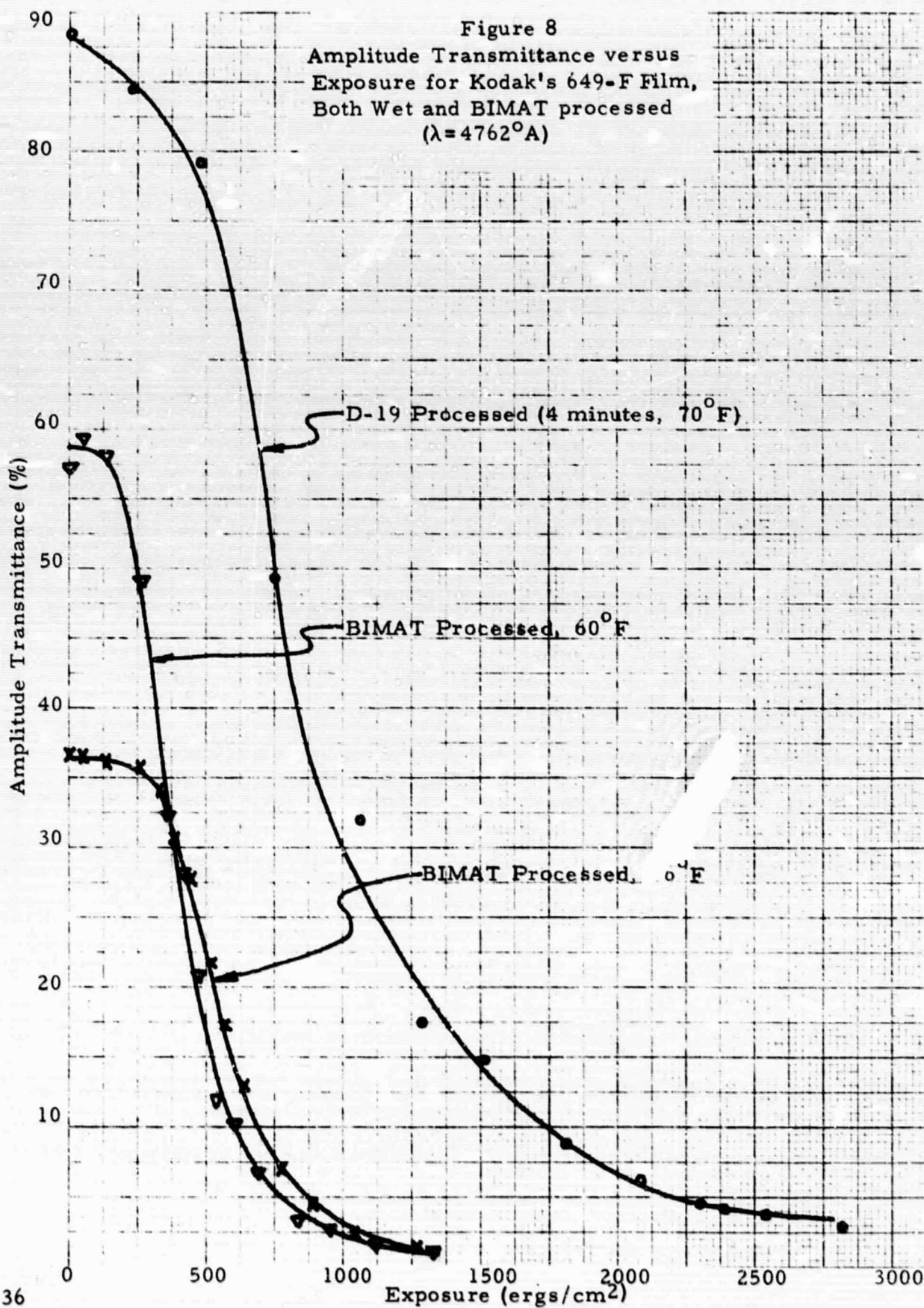


Figure 8
 Amplitude Transmittance versus
 Exposure for Kodak's 649-F Film,
 Both Wet and BIMAT processed
 ($\lambda = 4762^{\circ}\text{A}$)



as well as other films.

3.3.2 Film Noise Spectra

The Wiener spectra or power spectra of the complex film amplitude transmittance functions, as measured by the coherent optical spectrum analyzer described in Section 3.2.3, are plotted in Figures 9 through 15. All spectra were measured at the 4762⁰Å Krypton laser blue line. All films were in free space (no liquid gate was used), so the spectra are the result of film thickness variations, index of refraction variations, as well as film "grain noise." An attempt has been made to reduce the effects of the spectrum analyzer system noise by subtracting the system noise multiplied by the average intensity transmittance of the film, as described in Section 3.2.3.

The ordinate of each plot is the ratio of two light levels: The light power transmitted by a small aperture with an area of [1 line/mm]² in the Fourier transform plane, divided by the light power incident on the uniformly exposed negative. Spectra were plotted for several average transmittance levels for each film being investigated.

The film noise spectra for the free radical and dry silver films are given in Figures 9 and 10. At high spatial frequencies, the dry silver film is 5 or 6 times noisier than the free radical films. The noise characteristics of the two films are more nearly equal at lower frequencies, and the low transmission Dry Silver frame has less noise than the Free Radical low transmission frame for frequencies below about 170 lines per millimeter.

Two spectra for BIMAT processed SO-243 film are shown in Figure 11. The noise is generally comparable to the free radical noise level at high spatial frequencies, and three or four times lower for SO-243 at frequencies below 200 lines per millimeter. For comparison, spectra are shown in Figure 12 for conventionally processed SO-243 (D-19, 4 minutes, 70⁰F). The noise levels are comparable at 30 to 40 lines per millimeter, but the

Film 9 - Film Noise Spectra for Photo Horizon's
Free Radical Film ($\lambda = 4762^{\circ}\text{A}$)

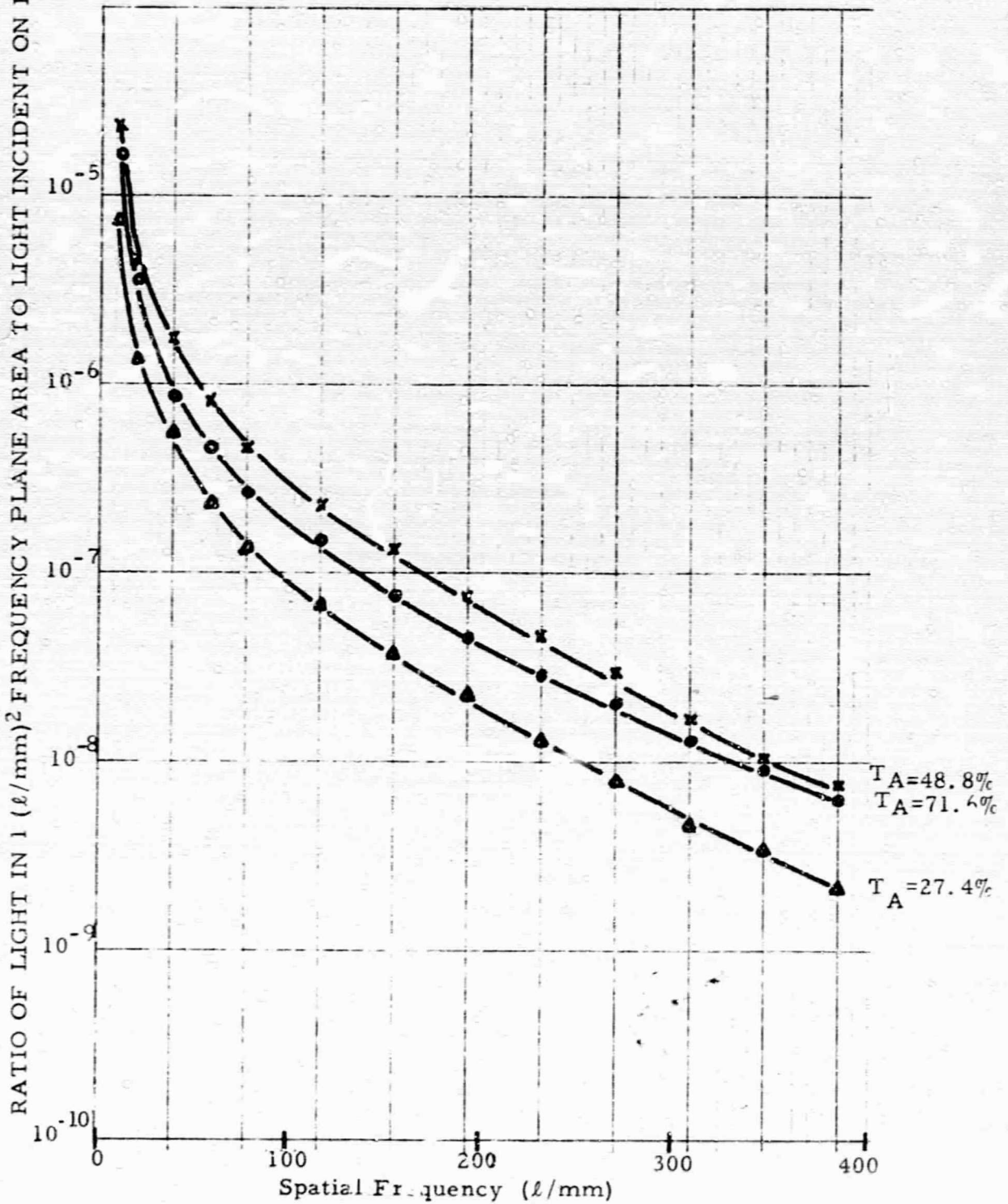


Figure 10 - Film Noise Spectra for 3 M's
 Dry Silver Film ($\lambda = 4762^{\circ}\text{A}$)

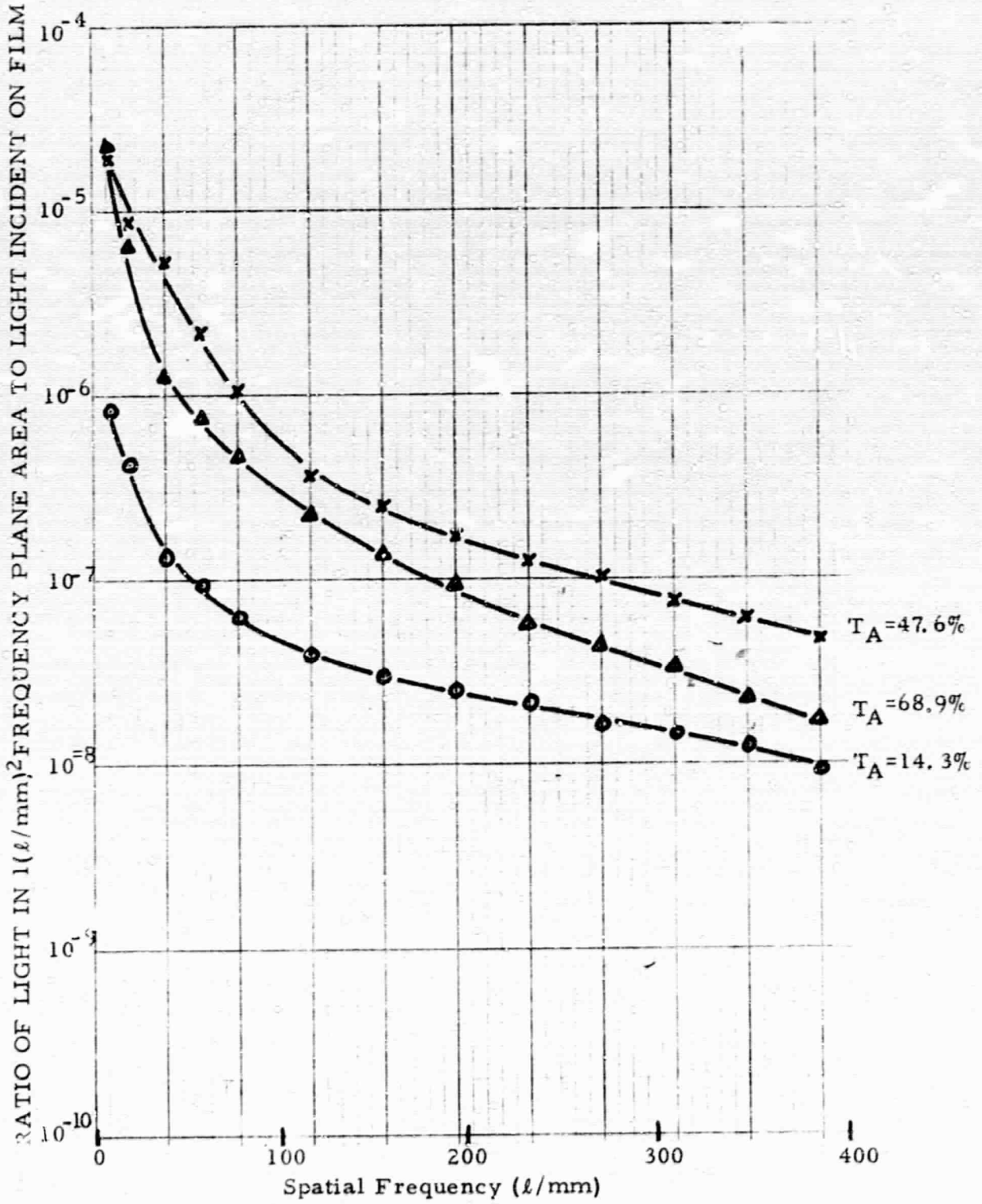


Figure 11 - Film Noise Spectra for Kodak's SO-243 Film
 Processed with a BIMAT Film ($\lambda = 4762^{\circ}\text{A}$)

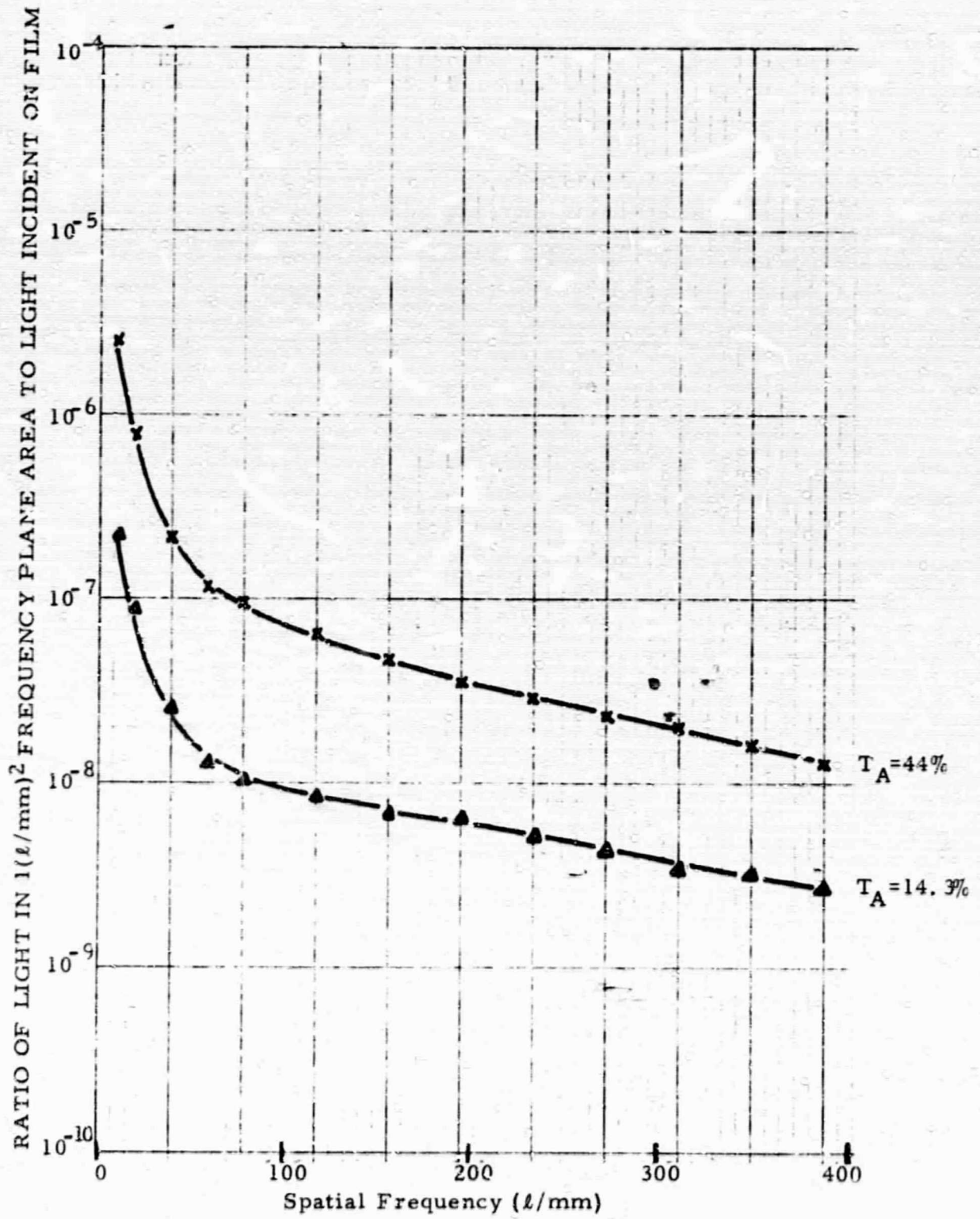
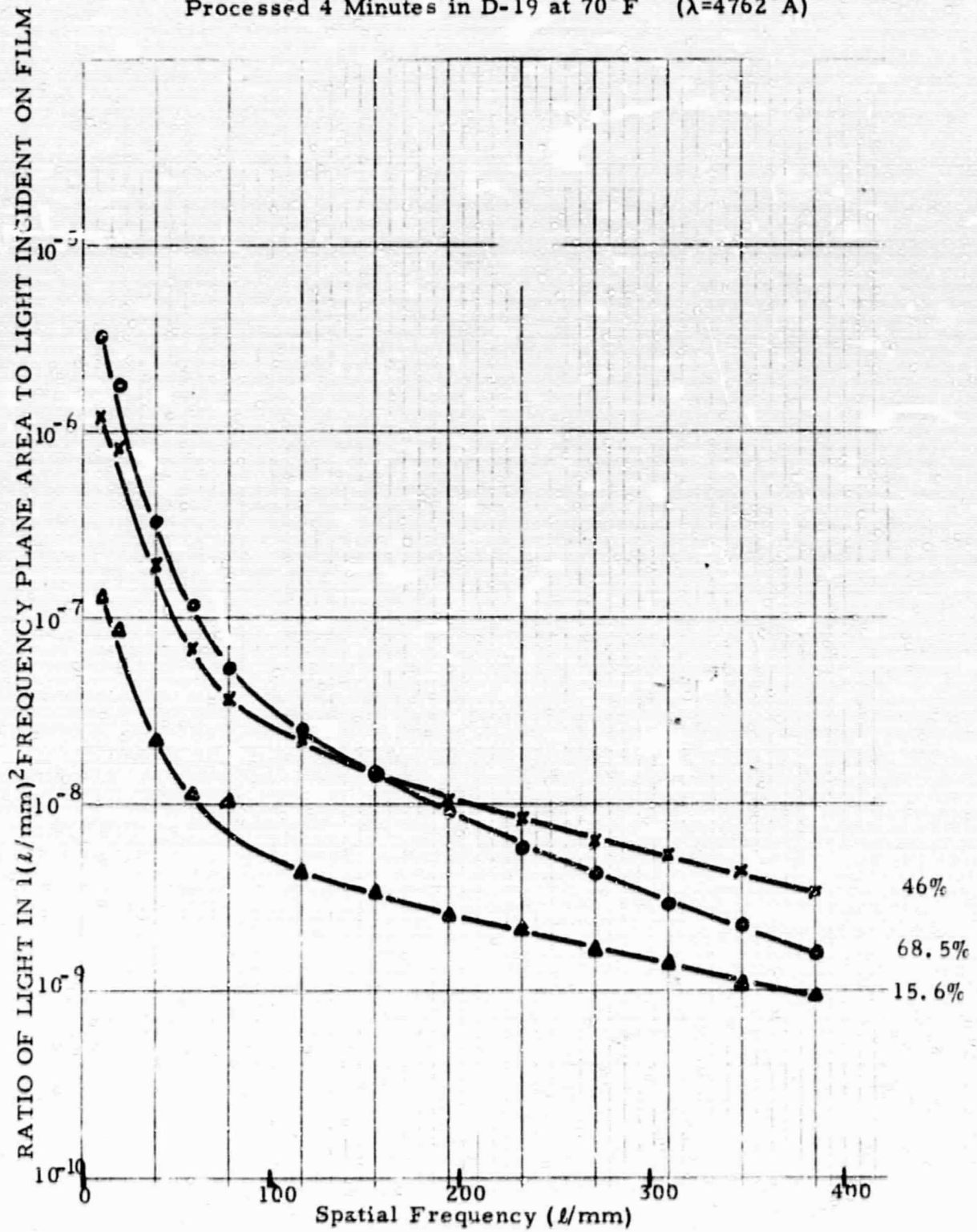


Figure 12 - Film Noise Spectra for Kodak's SO-243 Film
 Processed 4 Minutes in D-19 at 70°F ($\lambda=4762\text{Å}$)



BIMAT processed film becomes up to 5 times noisier at higher spatial frequencies.

Similar noise spectral plots are given in Figures 13 and 14 for BIMAT and conventionally processed 649F film. Here the differences are more striking. The 649F film is one of the highest resolution, finest grain films manufactured. It is used extensively for holography and other special applications requiring resolution of several thousand lines per millimeter. Figure 14 therefore represents one of the lowest achievable film noise spectra. The BIMAT processing, however, increases the noise level by as much as 35 times over the wet processed 649F film. Note, however, that this BIMAT chemistry was designed for use with SO-243 type films, and may not be optimum for processing 649F films.

The results of the BIMAT versus wet processed films are summarized in Figure 15. The spectra for SO-243 and 649F processed to an amplitude transmittance of approximately 50% are shown for BIMAT and for wet processing. Notice that the BIMAT process actually generated slightly more noise on the 649F film than on the normally coarser grained SO-243 film.

Figure 15 also permits us to make a crude comparison between the power spectrum versus the "RMS granularity" measure of film noise. The comparison would be more meaningful if the spectra were measured with the films in a liquid gate, since the RMS granularity is little affected by phase noise, while the power spectrum is affected. Nonetheless, at high spatial frequencies and amplitude transmissions near 50%, the grain noise should be predominant in the spectral data. Over much of the spectrum, the wet processed SO-243 is about 5 times noisier than the wet processed 649F film. The published Eastman Kodak data gives an RMS granularity of 7.4 for SO-243 and 4.7 for 649F¹⁸, which is a ratio of only 1.57. Thus, the power spectra show a much wider difference in film noise for this particular case.

One explanation for this difference in noise ratios is that the procedure for determining RMS granularity by scanning the film with a 48

Figure 13 - Film Noise Spectra for Kodak's 649-F
 Processed with BIMAT Film

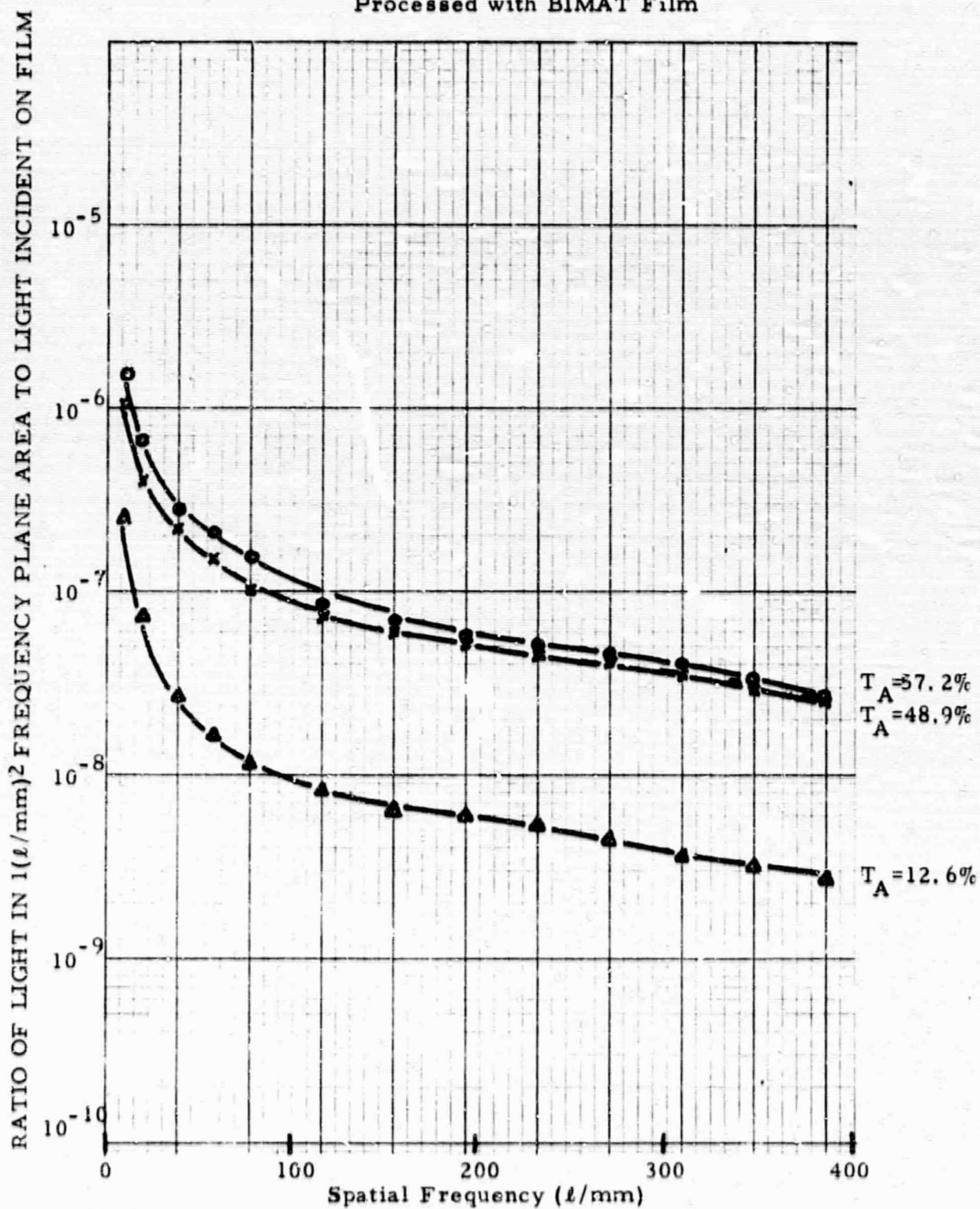


Figure 14 - Film Noise Spectra for Kodak's 649-F
 Processed 4 minutes in D-19 at 70°F ($\lambda=4762^\circ\text{A}$)

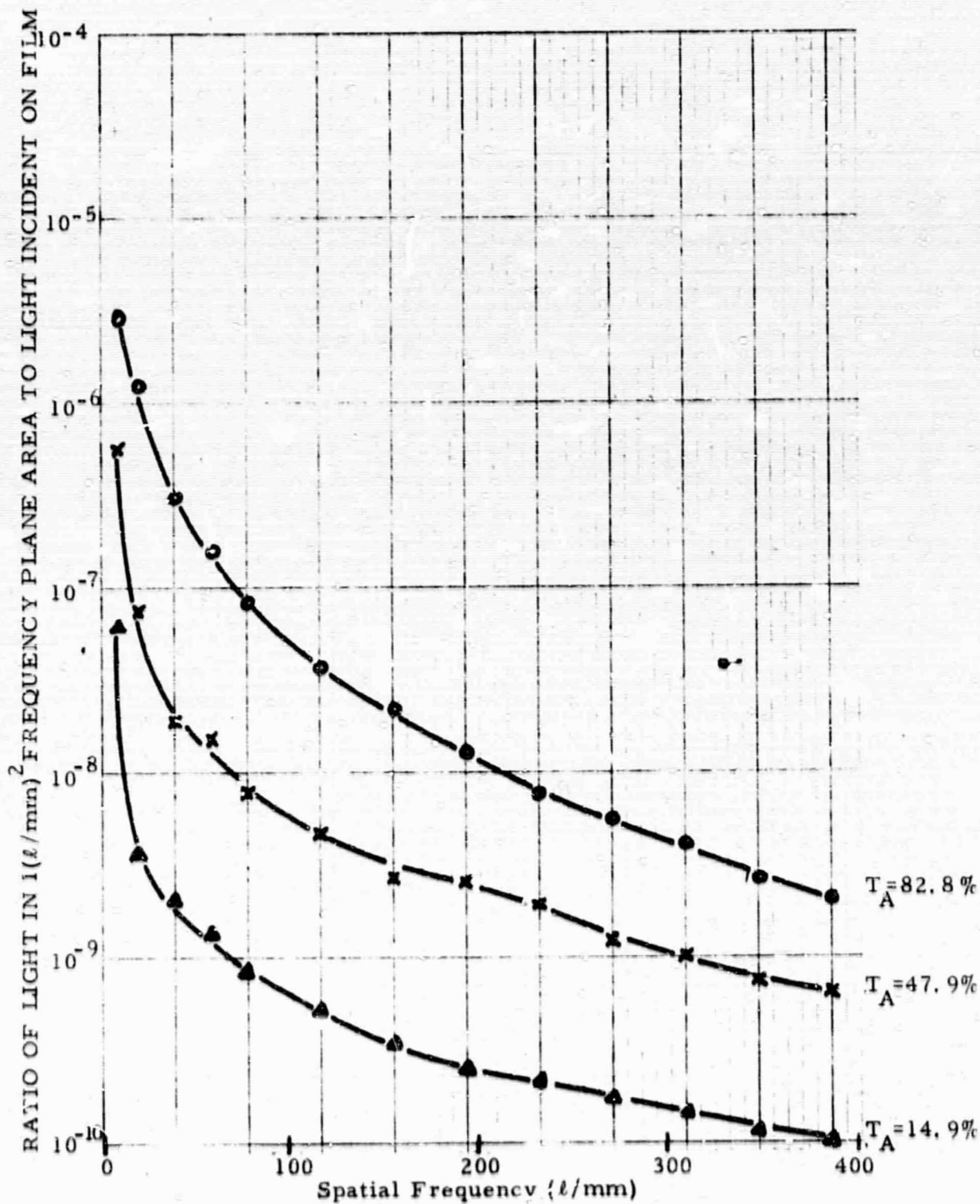
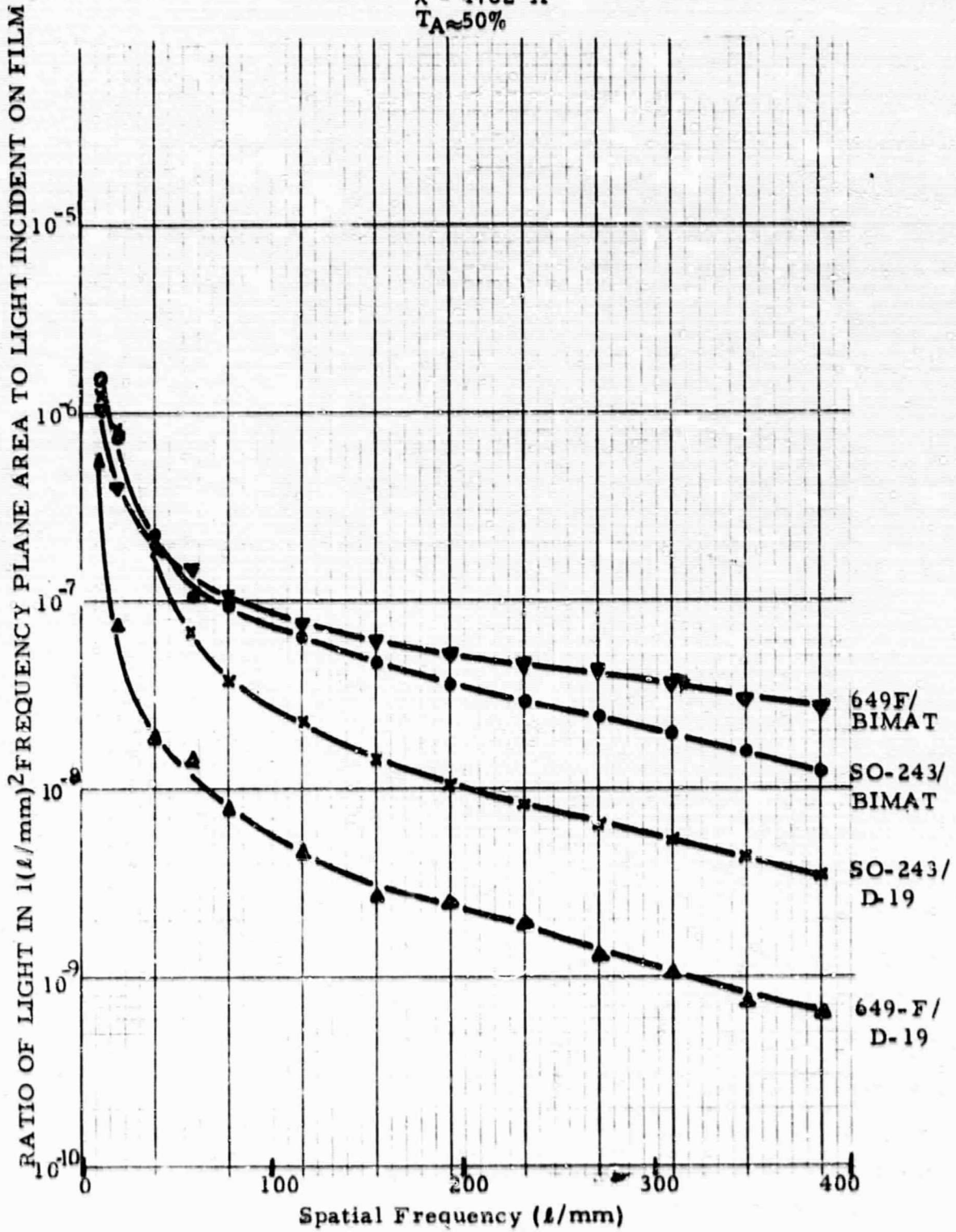


Figure 15 - Comparison of Film Noise Spectra
from BIMAT and Wet Processed Films

$\lambda = 4762\text{\AA}$
 $T_A \approx 50\%$



micron pinhole essentially discards the high spatial frequency information. That is, the scanning pinhole convolves the film (intensity) transmittance function with the pinhole. This averages out the high frequency data. By the convolution theorem, the frequency content of the microdensitometer time varying voltage will be the product of the film noise spectrum and the transform of the pinhole in one direction. The Fourier transform of a 48 micron pinhole will have a null in the vicinity of 20 lines per millimeter. Spatial frequencies much above 20 lines per millimeter will therefore contribute very little to the RMS granularity measurement.

Referring to Figure 15 again, the lowest spatial frequency data point is near 10 lines per millimeter. Here SO-243 is only about 2.6 times noisier than 649F. This is much closer to the 1.57 ratio predicted by RMS granularity measurements. This is but one example of the inadequacy of RMS granularity for fully characterizing a photographic process.

Other factors which probably contribute to the different relative noise measures for these two evaluation methods include the sensitivity of the power spectra to film phase noise, the relatively little power spectral data available, and possibly the fact that the RMS granularity measurements are made at a density of 1.0. A density of 1 corresponds to an intensity transmittance of 10%, or an amplitude transmittance of 31.6%. At lower transmittances, the discrepancy is even higher. Our limited spectra do not include data near 31.6%, but in the vicinity of 15% amplitude transmittance, 649F noise levels approach one-tenth that of SO 243 at high spatial frequencies. At the lowest spatial frequency measured (9.7 /mm), the SO-243 noise spectrum level was about twice the 649F spectrum. Thus the discrepancy between the RMS granularity measure and the complete noise spectrum is apparently greater at lower amplitude transmittance, although more nearly comparable at very low spatial frequencies. These observations should be verified with more experimental data.

3.4 Summary Evaluation of Rapidly Processed Films

For most optical data processing systems requiring quasi-real time access to the developed film, the BIMAT process appears to be the best choice at this time. The BIMAT system is flexible, in that a fairly wide variety of negative films can be utilized to satisfy various system resolution and sensitivity requirements. The relatively long processing time (90 seconds to 20 minutes) is a major disadvantage of this technique.

For those applications which require access times of less than 20 seconds, either nonsilver halide films such as the Free Radical or Dry Silver films must be used, or else an elevated temperature wet processing of silver halide materials is required. The choice between Dry Silver and Free Radical film will depend on the application. Dry Silver is more sensitive, has better shelf life, and is processed in one step. Free Radical has slightly less noise at most spatial frequencies, has no reciprocity failure, and very excellent resolution. Both films will probably improve when better coating procedures are instigated.

3.5 Recommended Future Film Study Work

Under the existing contract we have become familiar with the characteristics of several unconventional rapidly processed photosensitive films, have set up reasonably accurate apparatus to measure important characteristics of those films, and have made a few preliminary measurements. Much more research is required both for the existing star correlator application, as well as for the general class of coherent optical data processing problems. Many additional film measurements are needed to increase the reliability of the data already collected and to investigate the dependence of film characteristics on other parameters, such as wavelength, temperature, shelf life, etc. In addition, a theoretical program should be started to develop operational models for the various photo processes so that we can predict the performance of optical processing systems. In the past, our inadequate knowledge of film characteristics (or improper application of what we

do know about films) has hindered the accurate analysis of optical system performance, particularly in coherent light.

Several specific tasks which should be instigated have been suggested by our investigations on this contract, as listed below:

Liquid Gate - All of the T_A -E and film noise measurements were made with the film attached to a metal frame. Time did not permit a repetition of these measurements with the film immersed in a liquid gate. Such a gate, which surrounds the film with a fluid whose index of refraction closely matches that of the film's emulsion, reduces the effects of film noise due to film thickness variations. Aside from yielding more information about the film's characteristics, this measurement task has very real importance since many optical processors utilize liquid gates to suppress film relief image noise. Film characteristics in a liquid are needed.

Wavelength Dependence - All of our measurements and exposures were made at the 4762°A Krypton laser blue line. The Krypton laser was chosen for this measurements program because its lines are fairly evenly distributed through the visible spectrum. We would like to measure the characteristics of these films at different wavelengths to determine if there is an optimum wavelength for reducing film noise or increasing effective linearity, etc. This wavelength dependence may exist both for exposure (which could affect the choice of wavelength for a laser recorder, for example), as well as for illumination of the processed film (which would guide the choice of a wavelength for the optical processor itself).

Other Films - This study should be expanded to cover several other films. The BIMAT process should be used on higher sensitivity films such as Kodak's Panatomic-X or Plus-X type films, as well as the new SO-382 film which has characteristics somewhere between SO-243 and 649F. The technical monitor on this contract has suggested that Polaroid films may be useful, and these should be included in any future study.

Improved Neutral Density Filters - One of the limitations to the accuracy of our film noise spectral measurement system was the wedge in our glass neutral density filters. Filters are essential in measuring the wide dynamic range of the film spectra, but any small wedge angle causes a change in the laser beam angle, which in turn shifts the focused beam relative to the input spatial filter pinhole. This varies the intensity of the light in an unpredictable manner, particularly when several filters are cascaded. Unfortunately, we could not obtain sufficiently high quality filters in time for this contract, but they should be used in any future experiments.

Verify Repeatability - While we have checked the accuracy of our optical equipment with many more measurements than are reported in this document, more data should be taken to verify and refine the accuracy our measurements. Once the accuracy has been well established, several films of each variety should be exposed under nominally identical conditions. The characteristics of these films should then be measured to determine the repeatability of the particular photosensitive process.

Parameter Variation - Parameters other than the light wavelength should be varied and their effect on film characteristics should be established. The temperature dependence of the fog level of BIMAT processed 649F has been identified. This temperature dependence should be studied in more detail. Can the fog level be reduced further by lower temperature processing? What is the effect of lower temperature processing on the noise spectrum? Is the BIMAT processing time to completion extended at lower temperatures and, if so, by how long? What are the effects of very short BIMAT processing times on the order of 10 to 30 seconds.

Similar questions can be asked of the Dry Silver and Free Radical processes. We have only investigated these two films under one fixed processing scheme.

Shelf Life - All three films investigated have a limited shelf life. In most cases the manufacturers do not describe what adverse effect would result from exceeding or approaching the recommended shelf life. A controlled study of sensitivity, fog level, and noise characteristics should be undertaken for samples of each film stored at different temperatures.

Vacuum Operation - For space applications the performance of each film should be investigated in a vacuum. While special equipment would probably be required to expose the test films in a high vacuum (e. g., a good quality window access to the vacuum chamber, etc.), these vacuum experiments are necessary for any contemplated space mission. Horizons Research has reported a 15 times improvement in sensitivity of a Free Radical film in the absence of oxygen (Ref. 6). Assuming no similar increase in the Dry Silver sensitivity in a vacuum, then these two films would have nearly equal sensitivity in space. Lewis and James (Ref. 19) have reported an increase in the sensitivity of conventional silver halide films in a vacuum, along with a reduction in low intensity reciprocity failure.

Theoretical Analyses - New mathematical models are needed for the photosensitive recording media used as inputs to a coherent optical system. With proper analysis of a film's T_A -E curve and noise spectrum, for example, we should be able to predict the input signal to noise ratios which can be tolerated in an optical correlator, the harmonic distortion and linearity of a spectrum analyzer, and the degree of restoration expected from an optical image enhancement system designed to remove motion, out-of-focus, or atmospheric turbulence degradations. One of the key elements of any successful mathematical model will be the rejection of the additive noise concepts so frequently encountered in the literature. Photographic noise (as well as the signal) is actually multiplicative, and thus depends on the signal level at any local area of a film. Any theoretical predictions which ignore these realities can at best be approximate solutions to a complex problem.

4.0 INTRODUCTION TO IMAGE INTENSIFIERS

High-gain, high-resolution, photoelectronic intensification is applied under conditions of low incident light levels or whenever the integration time required by a sensor or recording instrument exceeds the limits of practicability. Examples of such situations are (aerial) night reconnaissance, special radiography in medical or industrial applications and special film recording situations where conventional silver halide films are replaced by unconventional slower recording materials such as photochromics, thermoplastics, free radicals and other such recording media.

High-gain, photoelectronic image intensification may be achieved by several methods, some of which are listed below:

- (a) Cascading single stages by coupling lens systems
- (b) Channel-type, secondary emission image intensifier
- (c) Transmission secondary electron multiplication image intensifiers (TSEM tubes)
- (d) Direct electronographic intensification (Lallemand Electronic Camera)
- (e) Cascading of single stages enclosed in one common envelope.

Cascading single stages by coupling lens systems is quite inefficient as the lens system limits the obtainable gain severely. Channel-type image intensifiers are capable of achieving high gain values and are quite rugged; however, they suffer from inherently low resolution and high image noise characteristics as will be

described. TSEM tubes have been constructed showing high gain and resolution but are large, fragile, and require magnetic focusing. Severe resolution limitations are anticipated with electrostatic focusing due to chromatic aberrations. Furthermore, the thin dynodes have a natural diameter limitation whenever a mesh support cannot be tolerated for resolution reasons. The Lallemand electronic camera offers a unique photoelectronic image intensification system for space environment but requires development for application. This system will be discussed later.

Cascaded single stages enclosed by a common envelope have been the most extensively developed high gain, high-resolution image intensification systems. The electron optical system may be either magnetic or electrostatic with variable magnification.

An electrostatic focusing system generally suffers degradation due to image plane curvature leading to defocusing in the peripheral image region if a flat viewing screen (or interstage coupler) is utilized, while a magnetic system requires accurate adjustment of a solenoid which is heavy and bulky. As it will be discussed later, peripheral defocusing can be improved by utilizing curved fiber optical couplers. It should be noted that the paraxial resolution is quite similar for both electron optical focusing systems.

It is felt that the fiber-optic-coupled multistage (two) image intensifier is the best currently available photoelectronic image intensification system. Therefore, in this report we shall consider the theoretical gain and resolution capabilities of such tubes. The luminous efficiency and resolution of single stages, fiber couplers and finally the composite tube will be computed.

It will be shown theoretically that high image intensification obtainable with such a tube and contact or relay photography permits the utilization of extremely low light levels and long film integration times or conversely moderately low light levels and short film integration times (exposure). The effects of device and quantum noise, associated with low input levels, will be described.

In addition, theoretical considerations of matching the noise and signal to the recording film will be given for a specific recording technique.

The conclusion shall be obtained in this report that fiber-coupled double-stage tubes represent a sensible and practical approach to high-gain, high-resolution image intensification for direct film recording for short exposure times. Possible advantages of a theoretical two stage Lallemand "direct electronographic" system will be presented.

4.1 Fiber-Coupled Double-Stage Image Intensifier

The tube design which forms the basis of this theoretical discussion is a two stage electron optical system based on the focusing action of concentric spherical cathode and anode surfaces²⁰. The inner (anode) sphere is a pierced, elongated cup, and terminated by the phosphor screen. The photoelectrons emitted from a circular segment of the cathode sphere are focused by the positive lens action of the two concentric spheres, pass through the negative lens formed by the anode aperture, and impinge upon the cathodoluminescent viewing screen. The cylindrical focusing electrode permits adjustment of the positive lens part by varying the focusing potential. The anode potential codetermines the gain G , and magnification M , of the stage.

Both the photocathode and the image plane of such an electrode configuration are curved concave as seen from the anode aperture. The field-flattening property of the biconcave fiber coupler can be utilized to alleviate the resolution losses resulting with a flat phosphor-screen or coupling member. For the same reason, the output fiber plate is planoconcave, its exposed flat side permitting contact photography if a permanent record is desired.

The second photocathode and both phosphor surfaces are deposited on the fiber plate substrates. The photocathode sensitivities S , phosphor efficiencies P , and anode potentials v , of the individual stages are distinguished in the report by subscripts I and II. Both stages are assumed to have unity (1) magnification M .

4.1.1 Theoretical Discussion of Flux Gain

The luminous gain G_L (ratio of total exit flux to total incident flux) with unity magnification is, to a first approximation, given by

the product of the photocathode sensitivity S (amp/lumen), the anode potential v (volts) and the phosphor conversion efficiency P (lumen/watt). In general P is a function of v , the anode potential and current density, but is nearly constant for applied voltages of 10 to 20 kilovolts per stage²¹ and shall be assumed constant here.

The luminous efficiency $S(\lambda) \equiv S_L$ of a photocathode depends on the maximum radiant sensitivity S_W^{MAX} and on the spectral distribution of the incident light flux $E(\lambda) \equiv E$ (watts per unit wavelength interval at wavelength λ) by the relation:*

$$S_L \left(\frac{\text{amp}}{\text{lumen}} \right) = S_W^{\text{MAX}} \left(\frac{\text{amp}}{\text{watt}} \right) \frac{\int ESd\lambda}{680 \int EVd\lambda} \quad (4-1)$$

where

$S \equiv S(\lambda)$ = the normalized radiant photocathode sensitivity

$V \equiv V(\lambda)$ = the standard visibility function

The luminous flux gain G_L of a single stage is given by

$$G_L \left(\frac{\text{lumen}}{\text{lumen}} \right) = \left(S_W^{\text{MAX}} \right) (v)(P) \frac{\int ESd\lambda}{680 \int EVd\lambda} \quad (4-2)$$

If the input light distribution falls beyond the visible range, $G_L = \infty$ since $\int EVd\lambda = 0$; such situations will not be considered here.

4.1.2 Fiber-Optical-Coupler Efficiency

The efficiency of fiber optics plates depends on four factors²²

* See Appendix A.

- (1) Numerical aperture (N. A.)
- (2) End (Fresnel Reflection) losses (R)
- (3) Internal Losses (I. L.)
- (4) Packing efficiency (F. R.)

The numerical aperture of fiber optical bundles is given by

$$\text{N.A.} = n_o \sin \alpha_i = \sqrt{n_c^2 - n_j^2} \quad (4-3)$$

where α_i is the acceptance angle, n_c is the index of refraction of the core glass, n_j is the index of refraction of the cladding and n_o is the index of refraction of the medium. Settled phosphors which are generally used as output screens have low optical contact and thus $n_o = 1$ can be assumed. The numerical aperture should, in general, be close to unity. When fibers of N. A. close to unity are used to transport light from or to a phosphor a certain fraction of the energy is refracted out of the fiber and contributes to the degradation of image contrast. The low index cladding helps reduce this effect.

A good approximation for determining the end reflection losses R can be obtained from the angle independent Fresnel formula

$$R = \frac{(n_c - n_o)^2}{(n_c + n_o)^2} \quad (4-4)$$

For phosphor to fiber and fiber to air (output) surfaces, assuming $n_c = 1.76$ and $n_o = 1.00$, we obtain $R = 7.5\%$. Hence, the $(1-R)$ factor for the output fiber coupler is given by $(1-R)^2$ (two surfaces) = 0.86.

Photosensitive surfaces of the SbCl_3 and multialkalide type have index of refractions of approximately 2. The Fresnel losses at the fiber-photocathode interface is about 0.5 percent and the $(1-R)$ factor for the interstage coupler is given by approximately 0.92.

The internal losses (I. L.) are due to absorption and small but finite losses suffered in the numerous internal reflections due to deviations from the prescribed cylindrical fiber cross-section and the minute imperfections of the core-jacket interface. These losses depend on fiber diameter and length, absorption coefficient, the mean value of the loss per interval reflection and the angular distribution of the incident light. Experimental data indicates that one can expect about 12% internal losses for 1/4-inch long, small (5-10 μ) diameter fibers²³. This is somewhat higher than the explicit expressions (integral averages) of about 3% to 6% per inch given in the literature. This relatively high value is probably due to small fiber diameters increasing the number of interval reflections.

The packing efficiency F. R. of fiber plates of circular fibers in a closely packed hexagonal array is given by

$$\text{F. R.} = 0.906 \left(\frac{d}{D} \right)^2 \quad (4.5)$$

where d is the fiber core diameter, D is the center to center spacing of fibers and 0.906 is the ratio of the area of a circle to that of the circumscribed hexagon. For the small diameter fibers which are now technically feasible i. e., $d = 5\mu$, the resolution is about 100 lp/mm as given by

$$R \cong \frac{1}{2d} \quad (4.6)$$

If we further assume a cladding thickness of 0.5μ the center to center spacing D is 6μ . Thus, using these numbers the packing efficiency is $F.R. = 0.63$.

Thus, the efficiency τ for each of the two fiber couplers ($\tau_I \equiv$ interstage coupler efficiency and $\tau_{II} \equiv$ output coupler efficiency) is given by

$$\tau_{I, II} = (N.A.)_{I, II} (1 - R)_{I, II} (1 - I.L.)_{I, II} (F.R.)_{I, II} \quad (4-7)$$

Now for the numerical examples given above

$$\tau_I = (1)(0.92)(0.88)(0.63) = 0.51$$

$$\tau_{II} = (1)(0.86)(0.88)(0.63) = 0.48$$

Now $\tau_T \equiv$ total efficiency is given by

$$\tau_T = \tau_I \tau_{II} = 0.25 \quad (4-8)$$

The image intensification system discussed thus far replaces the standard mica (glass) membrane interstage coupler and glass window-lens output coupler. For the sake of completeness let us compare the efficiency of this system with the one first described. Neglecting absorption, the end losses of the coupling membrane (mica interstage coupler) is 7% and the output window (output coupler, $n_w = 1.5$) is 8%. If we now use a relay lens (f/l) working at the 1:1 conjugate position (i.e., $M = 1$ unity magnification) the efficiency τ_L is given by (assuming unity transmission)

$$\tau_L \cong \frac{1}{4(f\#)^2 (M+1)^2} \cong 0.07 \quad (4.9)$$

The total efficiency τ_T of this system is given by

$$\tau_T = \tau_I \tau_{II} \tau_L = 0.06$$

Thus, we see that the fiber optic coupled system is about four times more efficient than the standard mica-lens system. The efficiency could be increased by putting the recording material in direct contact with the output window of this example but as we will see the resolution is so degraded that we do not consider this method.

4.1.3 Gain of Fiber Coupled Image Intensifiers

The overall luminous gain G_L of a fiber coupled double stage image intensifier including the possible brightness gain or loss ($1/M^2$) from area demagnification ($M < 1$) or area magnification ($M > 1$) is given by

$$G_L = \left[\left(\frac{S_W^{MAX} \int ESd\lambda}{680 \int EVd\lambda} \right) v_1 P \tau_I \right]_I \left[\left(\frac{S_W^{MAX} \int ESd\lambda}{680 \int EVd\lambda} \right) v_2 P \tau_{II} \right]_{II} \left(\frac{1}{M^2} \right) \quad (4.10)$$

It is obvious that careful choice of photocathode which maximizes the integral $S_W^{MAX} \int ESd\lambda$ for a given input spectral power flux E , for both stages is very important. This same consideration should be given to the second-stage phosphor screen for matching with the spectral sensitivity of the ultimate sensor (e. g., photographic emulsion).

The "matching integrals" for two types of photocathodes (S-11 and S-20) and two types of light input have been evaluated. The input light distributions considered are P-11 and "night light" (NL) as given by H. W. Babcock and J. J. Johnson²⁴. This night light corresponds approximately to a night sky spectral power distribution. The integrals are given in Table I below.

Table I. Matching Integrals*

| INPUT INTEGRAL | NL | P-11 |
|-------------------------|-----|------|
| $\int EV d\lambda$ | 548 | 166 |
| $\int ES_{11} d\lambda$ | 511 | 830 |
| $\int ES_{20} d\lambda$ | 750 | 800 |

Now using equation (4-10) and the parameters discussed previously, the luminous gain, G_L , for the possible combinations of S-11 and S-20 photocathodes and P-11 phosphor screen with P-11 and night light (NL) inputs are calculated and shown in Table II. The following efficiencies obtained from RCA specifications were used.

$$S_{W11}^{\text{Max}} = 50 \text{ m amp/watt} \quad P_{11} = 36 \text{ lumens/watt (aluminized)}$$

$$S_{W20}^{\text{Max}} = 64 \text{ m amp/watt}$$

The luminous gain values were computed using equation (4-10) with $v_1 = v_2 = 20\text{KV}$, $M = 1$, $\tau_I = 0.51$ and $\tau_{II} = 0.48$.

*Values taken from reference 37

Table II. Luminous Gain Characteristics

| Input Light | II STAGE | | $S_{20} - P_{11}$ | $S_{11} - P_{11}$ |
|-------------|-------------------|--|-------------------|-------------------|
| | I STAGE | | | |
| NL | $S_{20} - P_{11}$ | | 5760 | 4630 |
| | $S_{11} - P_{11}$ | | 3040 | 2440 |

There are a whole host of other output phosphor screens which could have been considered besides the P_{11} screen, but it is particularly attractive because it produces a brilliant actinic output widely used for photographic recording and has a short (30 μ sec) persistence. Obviously for other types of recording media a different phosphor, more suitably matched to the spectral characteristics of the recording material, would be required. Along this same line, some of the more exotic photocathodes such as ERMA (Extended Red Multi Alkali) and Ga-As photocathodes could be considered.

4.1.4 Theoretical Discussion of Paraxial Device Resolution

The resolution limitations for a single stage are given by the inherent resolution of the electron optical system as well as the resolution capabilities of the cathodoluminescent viewing screen.

The resolution capabilities of an electrostatic system depend on both the choice of magnification and chromatic aberrations. The chromatic aberrations depend on the chosen anode voltage and in general higher voltages produce less chromatic aberration, thus increasing the obtainable resolution.

Electrostatic systems of the kind described here have been tested for resolution capabilities by applying electronography. An upper limit appears to be in excess of 100 line-pairs per millimeter²⁵.

The inherent resolution of a cathodoluminescent phosphor screen decreases with increasing aggregate thickness (i. e., increasing anode voltage), decreases with decreasing porosity, and is impaired by the normally used aluminum mirror (factor of two gain in brightness). Thus, in general, particle size, light scatter, and electron scatter determine the obtainable resolution limit. Induced photoluminescence due to "Bremsstrahlung" in the phosphor screen is small for electrons under 30 kev (i. e., anode voltages less than 30 KV).

Settled cathodoluminescent phosphor screens (P_{11} ; P_{20} , etc.) have limiting resolutions of 80 to 100 lp/mm at anode voltage values of approximately 30 KV. For the following discussions we can assume electron optical resolution of 100 lp/mm and phosphor screen resolution of 100 lp/mm. It should be noted that special purpose transparent (nonaluminized), polished, nonscattering, low luminous efficiency, low noise phosphors (P_{11}) have been developed for high resolution PPI and CRT recording. These special phosphors have resolution limits of up to 500 lp/mm, but are down an order of magnitude in luminous efficiency. However, it must be recognized that improvement in resolution can only be significant in overall performance if the efficiency resolution product remains high (i. e., the deposited phosphor should have an efficiency not too far below fine grained P_{20} phosphors ($ZnCd5:AgCl$) of about 80 to 90 lumens/watt).

The major factor influencing the obtainable fiber optic coupler resolution is the center-to-center spacing, D . Since fibers are arranged in closely packed arrays (Hexagonal close packs), the closest line separation is the height of the equilateral triangle with sides D , or $0.75 D$. Thus the resolution (lp/mm with D in microns) is

$$R = 578/D \text{ (lp/mm)} \quad (2-11)$$

If $D = 6\mu$, then $R \cong 100$ lp/mm and as will be shown, this high resolution is necessary to avoid limiting the overall resolution of system by coupler resolution. This expression is correct if and only if the object distance is less than or equal to D . The resolution deteriorates rapidly if this condition is not fulfilled. Irregularities of the fiber plate may also lower resolution locally. It should also be noted that when the test object is just above the limit of resolution an orientational resolution phenomena is observed in that there are only three positions corresponding to the lines joining the centers of the fibers where the lines of the test object are resolved.

The overall resolution of a device containing several resolution-limiting components can be estimated assuming each individual resolution value is given by a square wave response. A number of theoretical approaches have been made in order to estimate the loss in information (resolution) by cascading optical elements. Obviously the most informative is the MTF for the final output stage but since this is an experimental result we shall use an empirical expression commonly used to obtain the total resolution, R_T , of cascaded optical systems; that is

$$\left(\frac{1}{R_T}\right)^2 = \sum_{i=1}^n \left(\frac{1}{R_i}\right)^2 \quad (4-12)$$

where R_i are the resolution limiting components. This quadratic addition is valid only in the case of statistically independent variables. The validity of this assumption is particularly questionable for fixed fiber coupler plates since there is a systematic error introduced at every point.

For the tube under consideration, the resolution-limiting components are the electron optics (a limiting resolution of 100 lp/mm is assumed per stage), the settled phosphor screen (100 lp/mm per stage) and the two fiber optic couplers (100 lp/mm per stage). The resulting effective resolution for the total system is 41 lp/mm. If we double the resolution of the fiber couplers (200 lp/mm) the system resolution is 47 lp/mm. If we remove the resolution limitation of the fiber coupler the maximum resolution is given by 50 lp/mm. Thus we see that the coupler plates are not seriously limiting the total system resolution.

In the case of glass or mica-couplers the spreading of a light spot through the coupler (thin glass or mica sheet) equals roughly twice the thickness of the membrane. Thus the resolution of the phosphor screen (100 lp/mm) would be reduced to 33 lp/mm if a membrane thickness of 5μ is assumed. Now using a simple output window (same thickness) and a lens coupler to the ultimate sensor (film) we can assume the lens introduces no further degradation. For this system the total resolution is 22 lp/mm.

The efficiency and (paraxial) resolution characteristics of four possible combinations can now be compared as shown in Table III.

Table III. Resolution Efficiency Characteristics

| Interstage Coupler | Output Coupler | Total System Efficiency | Paraxial Resolution (lp/mm) |
|--------------------|----------------|-------------------------|-----------------------------|
| Mica | Window-Lens | 6% | 22 |
| Fiber | Window-Lens | 3.3% | 28 |
| Mica | Fiber | 44% | 23 |
| Fiber | Fiber | 25% | 41 |

It should be noted that the peripheral resolution may be expected to be about the same with fiber interstage couplers (due to field flattening) but will be essentially lower with the plane-parallel mica sheet. Factors of two improvement in resolution have been obtained in classified image intensifiers.*

4.1.5 Device and Quantum Noise Limitations

The vacuum photoelectronic image intensifier is a relatively low noise device. Possible sources of noise are:

- (a) Field emission from photocathode and/or other tube components
- (b) Ion bombardment induced secondary electron emission from the photocathode (Ion Spots)
- (c) "Bremsstrahlung" giving rise to spurious fluorescence and photoelectron emission
- (d) Thermionic emission from the photocathode.

*Private Communication, RCA

Spurious electrons created by any of these processes may reach the phosphor screen and contribute directly to the noise level, or they may create luminescence from the glass of the tube envelope causing spurious photoemission from the photocathode. The first three sources of noise [(a), (b), and (c)] may be sufficiently reduced or fully eliminated by careful design and processing of the tube. The thermionic emission contributes under such circumstances 75 to 85 percent of the device noise. The thermionic emission for S-11 and S-20 photocathodes is about 80 to 120 electrons/in²-sec (10^{-17} amp/cm²) and can be further suppressed by cooling. Typically this noise level (2000 electrons/sec; total noise photoelectrons for a 10 cm² input area) is less than the minimum input signal as limited by quantum noise considerations. It should be noted that ion spots are particularly objectionable since they produce large luminous spots on the output screen which can and do mask signal detail.

When working at optical frequencies, detectors are subject to quantum effects. These effects will be most evident at minimum levels of detectivity, which will be evident at small numbers of received photons per measurement interval. The random arrival of photons when we are dealing with small numbers of photoelectrons per measuring unit can be described by the Poisson distribution. For large numbers of photoelectrons (photons) per measuring unit the Poisson distribution approaches the binomial distribution and either can be used. If N is the number of photoelectrons (minimum number of information carrying quanta or particles anywhere in the device) emitted from one resolution element, A_R , of the photocathode in exposure time, t , then the noise or fluctuation in the signal is given by \sqrt{N} . The signal to noise ratio (SNR) is given by

$$\text{SNR} = \frac{N}{\sqrt{N}} = \sqrt{N} \quad (4-13)$$

For small numbers of photoelectrons per measuring unit, which is the important case in matters of receiving sensitivity, one must use the Poisson distribution and the concept of error rate rather than signal to noise ratio in order to obtain meaningful results. It has been shown that this expression is given by⁷

$$P(M, \eta N) = \frac{(\eta N)^M e^{-\eta N}}{M!} \quad (4-14)$$

where $P(M, \eta N)$ is the probability that M photoelectrons will be produced when an average of N photons fall on a photoemitter surface with quantum efficiency η . For image intensifiers with luminous gains, G_L , of 1500 or better, single photoelectrons emitted from the input photocathode give rise to detectable outputs. This is really fluctuation noise due primarily to random thermal emission of photoelectrons by the input photocathode. It is larger than true "photon noise" because the cathode quantum efficiency is sufficiently low resulting in much smaller numbers of photoelectrons than incident photons and a greater relative fluctuation in photocurrent, than in photon-arrival rate.

N can be calculated from the photocathode illumination, L (foot candles; lumens per square foot) and the quantum efficiency of the photocathode, S_Q (electrons/photon), for an integration time, t , by the equation

$$N = L t Q S_Q A_R \quad (4-15)$$

where Q is the lumen to photon per second conversion factor given by

$$Q \frac{\text{photons}}{\text{sec lumens}} = \frac{\int E d\lambda}{680 hc \int E V d\lambda} \quad (4-16)$$

and

$$S_Q \frac{\text{electrons}}{\text{photon}} = S_W^{\text{MAX}} \frac{\int E S d\lambda}{\int E \lambda d\lambda} \frac{hc}{e} \quad (4-17)$$

where h is Plancks constant, c the velocity of light and e the electronic charge.

The factor A_R is given by

$$A_R [\text{ft}^2] = \frac{1.076 \times 10^{-5}}{4 r_c^2} \quad (4-18)$$

where r_c (lp/mm) is the maximum photocathode resolution of the system*. Thus the expression for N is given by

$$N \frac{\text{photoelectrons}}{\text{resolution element}} = \frac{2.47 \times 10^{10} L t S_W^{\text{MAX}} \int E S d\lambda}{r_c^2 \int E V d\lambda} \quad (4-19)$$

If we now plug in the values for the matching integrals for night light (NL) with $r_c = 41$ lp/mm and an S-20 input photocathode, the number of photoelectrons per second per resolution element is given by

$$N \cong 1.3 \times 10^7 L^{**} \quad (4-20)$$

Thus for this spectral distribution of input light, 10^{-7} foot candles corresponds to approximately one photoelectron per second per resolution element on the photocathode with a signal to noise ratio of unity.

*Actually r_c is the photocathode resolution as determined by the total system resolution [41 lp/mm for the previous example].

** Where L is the luminous flux

Typically, image intensifier tubes are specified by their radiant response characteristics in terms of the maximum equivalent screen background input defined as that value of coincident radiation at a specified wavelength (usually the wavelength of peak sensitivity of the photocathode) required to cause an increase in screen brightness equal to the screen background brightness. The screen of a cascaded image intensifier tube has a residual brightness (screen background) even when the input photocathode of the tube is shielded from all radiation. In an ideal tube this residual brightness would be caused by thermionic emission from the first photocathode. A typical multialkali cathode with thermionic emission of 10^{-17} amps/cm² at room temperature (22°C), a cathode sensitivity of 64×10^{-3} amperes per watt and a radiant flux gain of 50, has a resulting screen background of 8×10^{-15} watts/cm². Measured screen backgrounds are more typically from 10^{-13} to 10^{-14} watts/cm² due to field emission and ion feedback. This corresponds to considerably less than one photoelectron per resolution element. Fortunately screen background decreases much more rapidly than gain when the accelerating voltage is reduced so that for very low levels of incident radiation, it is possible to obtain improved contrast at the expense of image brightness.

4.2 Continuous Channel Multiplier Plates

Continuous channel multiplier plates for imaging applications are a result of fabricating two dimensional arrays of single channel electron multipliers.

4.2.1 Theory of Operation

The continuous channel multiplier is in theory a very simple amplifying device; it consists only of a high-resistance hollow pipe with a static electric field along the axis of the tube. An electron (from the photocathode) striking the wall of the channel will liberate secondary electrons. The liberated secondaries are accelerated down the channel by the electric field colliding with the channel liberating more secondary electrons. In this fashion, multiplication is accomplished, provided that the effective secondary emission ratio of the wall surface is sufficiently large. The gain depends upon the applied potential, the secondary emission characteristics of the channel wall and the ratio of the length to diameter of the channel. Typically the gain is adjustable (voltage) from a few thousand to as high as 10^8 .

Since the gain does not depend upon the absolute size of the channel (only ratio of length to diameter) of the channel, the dimensions may be scaled without affecting performance, and honeycomb arrays (hexagonal close packs) of parallel channel multipliers, called channel plates may be constructed. The channels are usually made from special glasses which are internally coated for electrical conductance properties. The actual manufacture technique is similar to those used for fiber optics.

A typical channel plate amplifier is constructed by first arranging the single channel electron multipliers in a matrix (hexagonal close pack). The bundle is sliced and polished into disks to give the proper ratio of channel length to diameter. Then an input photocathode and output phosphor screen are attached in a vacuum envelope about the channel disk. The application of a potential between the disk electrodes now allows the device to operate as a photoelectric image intensification device.

4.2.2 Performance of Channel Plate Amplifiers

If the trajectories of all electrons were simple, the continuous channel amplifier would be a nearly perfect multiplier. The secondary emission ratio and trajectories of individual electrons are statistical quantities and, hence, exhibit fluctuations. These quantities manifest themselves as undesirable noise in the multiplier. Five major sources of noise are:

1. Normally observed variation of the secondary emission ratio δ
2. Variation in δ due to the variations in the surface constants
3. Variation in δ due to field irregularities
4. Variation in δ due to variation in the angle of emission
5. Variation in δ due to variation in emission velocity.

The first of these noise sources includes such effects as variation of δ due to the variation in the angle of incidence of the primary electron and variation in δ due to imperfections in the "perfect surface" (i. e., pure homogeneous surface). The next two items depend on the state of art improvements in continuous channel multiplier fabrication. The last two items (4, 5) constitute the real fundamental effects which place a lower limit on the noise.

For currently available channel multiplier arrays*, total light efficiencies of 54%, resolution of 15 lp/mm, and electron gains of 10^3 to 10^8 are feasible. The loss of information in these channel plates is a significant factor which limits usefulness where presentation of input signal-to-noise is of ultimate importance. The very high electron gain, air stability, and robust character of this device does make it attractive for some applications; however, film recording of star fields is not currently one of them.

*Mullard (England); Channel Electron Multiplier Array G40-40S
(developmental, 1969)

4. 3 Direct Electronographic Intensification

People have for many years been concerned with producing the ideal photon detector, defined as one which correctly records all photons arriving at an image plane with a time-scale as long as may be required.

This can be approximated by combining a photoelectric surface with an electron-optical system and a suitable electron detector. The essential conditions are that:

1. The quantum yield of the photosurface must be high
2. The electron-optics must not sensibly decrease the resolution-contrast in the final image as compared to the original input object.
3. The electron detector must be able to record the arrival point of a single photoelectron in a recoverable form.

The first two conditions are usually fulfilled in image intensifiers; the third is more difficult to realize and usually lacking in these devices.

4. 3.1 The Lallemand Electronographic Intensifier

The Lallemand²⁷ electronic camera is a "direct electronographic" system in which a photocathode, an electrostatic (magnetic) lens system, and a photographic plate are introduced into a single evacuated chamber. There are no intermediary film, phosphors, or electronic amplifiers between the photocathode and final receptor (film) to degrade and distort the information provided by the photoelectric surface. Consequently, the Lallemand electronic camera has the following characteristics.

(A) Speed

Each photoelectron produces a track in the photographic emulsion (i. e. , approximately 10 grains of silver with a track length of 10μ for Ilford G5 plates at 50 KV). Thus, the speed depends only upon the quantum efficiency of the photoelectric surface. For example, in classical photography, where the exposure is made directly by photons, the information is limited by the number of photons (N) multiplied by the efficiency (p_f) of the photographic emulsion. The efficiency of a photographic emulsion, p_f , defined as the number of photons per grain for exposure, is difficult to evaluate but a value near 1.7×10^{-3} has been measured²⁸. Now in the case where the accelerated photoelectrons strike a film emulsion directly each electron is able to expose many photographic grains [the number is dependent on the energy of the electron (kev)]. The information in the picture should be approximately limited (except for the statistics in the number of grains produced per electron) by the information in the number of photons (N) received multiplied by the efficiency of the photocathode (p_c) [$p_c = 0.25$]. Thus the gain of this method over classical techniques is given by the ratio

$$\frac{Np_c}{Np_f} a = \frac{p_c}{p_f} a \cong 120 \quad (4-21)$$

where (a) is a statistical factor²⁹ to correct for the statistical distribution of grains produced per photoelectron. Consequently the gain inefficiency should be over 100 when the best photocathodes are employed. This factor could be increased by inserting a TSEM dynode (small resolution loss) amplifier of Ga-As-P where the secondary emission gain is 30 and a total gain of over 3000 could be expected.

(B) Resolution

In practice the axial resolution has been limited by the length of electron tracks in the film emulsion and not the electron-optics. For a 10μ track this would correspond to approximately 50 lp/mm. Kodak Maximum Resolution plates have obtained resolutions better than 80 lp/mm using this technique.

(C) Discrimination

Owing to the higher quantum efficiency of the photoelectric surface and the fine grain of direct electron beam recording films the electronographic camera is able to discriminate fainter source against a bright background than is possible using classical photographic techniques.

(D) Linearity

Experiments have shown that the density change for electron recording is proportional to the number of incident electrons and hence to the intensity of the incident light. This linearity of response is maintained up to a photographic density of 3 (see reference 30). It is interesting to note that the effect of this response is to make the electronic plates appear "washed out" compared to ordinary photographs.

The conventional Lallemand tube does present some difficulties for general laboratory usage. The photocathode must be protected from residual gases trapped in the film emulsion since these gases will destroy the photocathode. For optimum performance the entire system must operate under conditions of high vacuum since air scattering of electrons will result in loss of resolution and increased noise (ion spotting). Methods and techniques of eliminating these problems are discussed in the literature³¹.

4. 3. 2 A Modified Electronographic Xerographic Image Intensification System

In order to circumvent the necessity of using conventional silver halide films, a novel direct recording electronographic Xerographic image intensification system is suggested. Basically this system would differ from the standard Lallemand camera in that "mylar" film would be used to store an electronic charge distribution characteristic of the input object. Carbon toner particles would then be distributed upon the "mylar film" and thermally fixed to supply the image.

The resolution recording capability of this method is theoretically fixed by the toner particle size. Currently 0.1μ particles are available. The resolution capabilities are somewhat degraded by the smearing or melting of the particles during the fixing process. A reasonable upper limit to the resolution capabilities is suggested at about 500 lp/mm (see reference 32). The temperature typically required for heat fixing is around 140°F . The ASA equivalent speed of this process is approximately ten (10) (ref 32). This situation could be helped by the use of TSEM dynodes of Ga-As-P where appreciable secondary electron gains could be anticipated. For space environmental conditions the vacuum requirement is easily satisfied and such a system could be easily implemented. Questions of actual system performance would have to be experimentally determined.

5.0 SYSTEM CONSIDERATIONS

The ability of photographic emulsion to store light is astounding; however, at low light levels long exposure times are required. In some applications the long exposure time is not practical and image intensifiers are needed to overcome this problem. In this section a detailed example of a system using a light amplifier and film recording output will be presented. The system to be considered consists of a Schmidt-Cassegrain objective which forms an image of a faint object in the night sky on the flat photocathode of an image intensifier tube. The transfer system shall consist of a relay lens (f/l) operating at the 1:1 conjugates which transfers the image from the output screen (P-11) to the film plane. The exposure time for the film recording stage will be 0.010 seconds. The objective of this section is to examine such an image intensifier system and predict its sensitivity when used under field conditions.

5.1 Optimum Sensitivity

The target we will consider is an unresolved point together with night sky (noise) which is to be imaged on the photocathode. Using a 15 cm diameter aperture and one meter focal length for the objective gives a geometric aperture of $f/6.6$. The effective solid angle of the objective is given by

$$\pi (\sin \theta)^2 = \pi (0.077)^2 = 1.85 \times 10^{-2} \text{ steradians} \quad (4-22)$$

where $\sin \theta$ is given by

$$\sin \theta = \frac{1}{2 f/\#} = 0.077 \quad (4-23)$$

Now if we assume the spectral radiance due to the diffuse night sky (airglow) is given by 3×10^{-10} watts per cm^2 per micron per steradian then the irradiance (I_N) on the photocathode for a 0.3 micron effective spectral bandpass (S-20) is given by

$$I_N \left(\frac{\text{watts}}{\text{cm}^2} \right) = 0.3 \text{ (microns)} 3 \times 10^{-10} \left(\frac{\text{watts}}{\text{microns cm}^2 \text{ sr}} \right) \quad (4-24)$$

$$\times 1.85 \times 10^{-2} \text{ (steradians)} = 1.66 \times 10^{-12} \text{ watts/cm}^2$$

If we now assume an output power gain (radiant gain G_W) of 10^5 the output (I_O) will be

$$I_O = 1.67 \times 10^{-7} \text{ watts/cm}^2 \quad (4-25)$$

If we also use an $f/1$ relay lens operating at the 1:1 conjugates with an exposure time of 0.010 seconds the noise energy density on the film is given by

$$E_N = 1.67 \times 10^{-7} \left(\frac{\text{watts}}{\text{cm}^2} \right) 0.06 \text{ (relay lens efficiency)} 10^7 \left(\frac{\text{ergs}}{\text{watt}} \right) 10^{-2} \text{ (sec)} \quad (4-26)$$

$$E_N \cong 1 \times 10^{-3} \text{ ergs/cm}^2$$

According to R. C. Jones³³ this is approximately the optimum background exposure to give maximum detectivity for point images on Kodak Royal-X Pan Record film (see Appendix B). The noise equivalent energy of this film is approximately 1.54×10^{-9} ergs per resolution element as with optimum pre-exposure.

The sensitivity of the instrument may be estimated as follows:
 The signal to noise required for the final image is assumed to be 5:1
 (ref 34). For Kodak Royal-X Pan film the detective quantum efficiency
 is 0.00895 (ref 33); thus using the relationship (Appendix B)

$$Q \text{ (detective quantum efficiency)} \equiv \frac{(S/N)_{\text{out}}^2}{(S/N)_{\text{in}}^2} \quad (4-27)$$

we see

$$\begin{aligned} (S/N)_{\text{in}} &= (S/N)_{\text{out}} / Q^{1/2} \\ &= (5) \frac{1}{(0.0085)^{1/2}} \\ &= 53 \end{aligned}$$

Thus the energy required for a detectable image (E_D) on Royal X
 film according to this criteria is given by

$$E_D = (53) (1.54 \times 10^{-9} \text{ ergs}) \cong 8.2 \times 10^{-8} \text{ ergs} \quad (4-28)$$

Using a transfer lens efficiency of 0.060, a radiant gain of 10^5 , and a
 110 cm^2 effective input aperture, the input irradiance (I_D) for
 0.010 second is

$$I_D = \frac{8.2 \times 10^{-15} \text{ joules}}{(0.06)(10^5)(110 \text{ cm}^2)(10^{-2} \text{ sec})} = 1.2 \times 10^{-18} \text{ watts/cm}^2 \quad (4-29)$$

This instrument threshold is equivalent to an irradiance from the target of 2.6 photons of 0.43 micron light per square centimeter per second. Note, the energy of 0.43 micron photon is given by

$$Q \left(\frac{\text{watts}}{\text{photon}} \right) = \frac{hc}{\lambda} = \frac{6.62 \times 10^{-34} \text{ joule-sec} \times 3 \times 10^8 \text{ meter/sec}}{4.3 \times 10^{-7} \text{ meters}} \quad (4-30)$$

$$Q = 4.61 \times 10^{-19} \text{ watts/photon}$$

It is evident that this estimate is unreasonable as it corresponds to approximately 3 photons per exposure or approximately one photoelectron per two exposures. We are temporarily neglecting tube noise. If we have a gain of 10^5 with a quantum efficiency of 0.2, then each effective photon is multiplied 5×10^5 times. With a transfer lens of 0.06 efficiency we would have 3×10^4 photons on the film for each photoelectron from the photocathode. The noise equivalent energy of Kodak Royal-X film is equivalent to 334 photons (0.43 micron) and a detectable image is 53 times this quantity or 1.77×10^4 photons. Thus the signal from a single photon (3×10^4) is well above this value and should be visible (detectable) without pre-exposure.

5.2 Noise Matching to Film

Let us now investigate the specifications of an instrument such that the gain of the image intensifier-transfer lens system is required to produce on film an exposure whose energy is equivalent to the rms granularity of the film for each photoelectron leaving the photocathode. This together with a suitable combination of objective focal ratio and exposure time to produce the optimum pre-exposure level with the sky background with little increase in rms granularity, will result in an instrument with the highest possible sensitivity and with maximum

dynamic range (on both tube and film) and maximum resolution. For Royal-X Pan film that has been pre-exposed uniformly to approximately 10^{-3} ergs/cm² the noise equivalent energy is 1.54×10^{-9} ergs. This noise equivalent energy is equivalent to 334 photons (0.43 microns). If we design a system so that the continuum exposure is again equal to the optimum pre-exposure, but each photoelectron event at the photocathode produces 334 photons at the film, the gain required is given by

$$G_R = \frac{(334)(0.2)}{0.06} \cong 1113 \quad (4-31)$$

which is the number of photons on the film per photon event at the photocathode multiplied by the quantum efficiency of photocathode and divided by the relay lens efficiency. The area associated with this number of photons (334) corresponds to a square 12.4 μ on an edge to correspond to R. C. Jones data.³² Since this (80 lp/mm) is considerably beyond the resolution expected (40 lp/mm) the noise figure for the background should not be increased unreasonably. Using a signal to noise of five the ultimate system sensitivity (I_u) is given by

$$I_u = \frac{(53)(1.54 \times 10^{-9} \text{ ergs})(10^{-7} \text{ watt/erg})}{110 \text{ cm}^2 (1113)(0.06)(10^{-2} \text{ sec})} \quad (4-32)$$

$$I_u = 1.1 \times 10^{-15} \text{ watt/cm}^2$$

This irradiance corresponds to 2,386 photons per square centimeter per exposure for 0.43 micron light. For a quantum efficiency of 0.2 and the aperture given, this corresponds to 477 photoelectrons from the photocathode for each exposure. The calculation to determine the signal to noise from the film is obscure in this case as the noise is not random in the sense it is in an ordinary photograph without a light amplifier. Thus treating the noise in the Poisson limit the noise in this case goes approximately as $1/\sqrt{477}$ or 0.046. Other sources of noise will raise this value somewhat. It would appear that this is the threshold of the instrument for quantitative estimates. On this basis it would seem that no more sensitive instrument could be built with a 15 cm aperture, a quantum efficiency of 0.2 and a 0.01 second exposure. This type of calculation can be applied to other film-light amplifier systems given the characteristics of the film and image intensifier.

A good approximation of the dynamic range of the intensifier is given by the ratio of the maximum light input power to the threshold light input power. Thus for the preceding, the dynamic range, DR, is given by

$$DR = \frac{10^{-8} \text{ watts/cm}^2}{10^{-15} \text{ watts/cm}^2} \cong 70 \text{ db}$$

where $10^{-8} \text{ watts/cm}^2$ is the expected damage threshold for S-20 photocathodes and P-11 phosphor for gains on the order of 10^4 . This recording dynamic range is obviously beyond the recording ability of typical films.

There are several problem areas that one might expect from image intensifiers based on previous experiments:

1. Image persistence; an image, either as a point or dispersed, remains on the tube screen for longer than quoted persistence times, due to internal screen fluorescence and phosphorescence, resulting in wakelike trails when the object is moved.

2. Bright targets; a bright target becomes surrounded with small luminous specks, believed to be caused by ions created by the interaction of the high density photoelectron beam with residual gas atoms.

3. Bright targets; the images of bright targets tend to be enlarged resulting in a loss of resolution. It is not clear whether this effect is due to the image intensifier or the film.

4. Mottle; individual photoelectrons leaving the photocathode are recorded on the film. The granularity is larger than the inherent film granularity and gives the picture a mottled effect, known in X-ray works as "quantum mottle".

5.3 Summary of Image Intensifier Investigation

Modern image intensifiers are capable of achieving high gain factors. The growing art of fiber optics offers the possibility of improved coupling between two or more stages without excessive gain or resolution loss, such as potentially encountered with lens or membrane couplers.

The theoretical gain of double stage image intensifiers, depending upon the performance of individual stages and the efficiency of the coupler was computed in detail. It was shown that image intensifiers with night light input and S-20 photocathodes should be capable of reaching gains as high as 10^4 . Utilizing fiber optics output couplers may increase coupling efficiency by a factor of 4 to 6 compared to a conventional lens system.

Resolution limitations as determined by the inherent phosphor-screen resolution, fiber diameter and electron optics have been described. It has also been shown that high-gain image intensifiers are essentially limited by quantum noise.

Continuous channel arrays have been discussed and compared in terms of gain, resolution, and noise characteristics.

The direct electronographic recording camera has been discussed in terms of its limitations and advantages. The Xerographic recording modification has been suggested but no reliability experimental data is available to substantiate the possible advantages the system offers over standard direct electron recording films other than its lack of chemical processing.

Finally, the concept of optimizing an image intensifier-film system has been discussed in terms of a detailed example. The concept of "detective quantum efficiency" and "equivalent film input noise" has been introduced as a set of parameters for maximizing the sensitivity and resolution of a total system for actual field operation.

The final conclusion appears to be that fiber optically coupled image intensifiers used in contact film recording situations offer the greatest resolution-sensitivity combination currently available.

6.0 EFFECTS OF IMAGE SMEARING DUE TO SPACECRAFT ROTATION

The immediate purpose of this study contract is to provide data for the design of a spacecraft attitude sensor based on coherent optical star correlation. The star field must be imaged onto the film, the film must be developed and correlated against a stored reference star map. If the spacecraft is spinning, however, the star image will be smeared on the film. In this section we consider the effects of this image smear on the correlation process.

In the following sections we will calculate the exposure time required for each film assuming no spacecraft motion; we will then calculate the maximum local exposure possible assuming a 4 rpm spin stabilized spacecraft, and then show that we require both smeared images and an image intensifier tube just to record on BIMAT processed SO-243 film. It will be shown that intentional smearing does increase the correlator signal to noise ratio linearly with the smear distance.

6.1 The Stationary Spacecraft Exposure Time

Consider a single star which produces an irradiance of I_s watts/cm² at the lens of the spacecraft camera. The camera will collect light power of

$$P_c = \frac{I_s \pi D^2}{4} \text{ watts.} \quad (6-1)$$

where D = the effective diameter of the collecting lens.

Assume that 50% of this light is concentrated in the diffraction limited area of

$$\frac{\pi \delta^2}{4} = \frac{\pi}{4} \left(\frac{\lambda f}{D} \right)^2 \quad (6-2)$$

The light irradiance exposing the film will be

$$I_f = \frac{2 P_c}{\pi \delta^2} = \frac{D^4 I_s}{2 (\lambda f)^2}. \quad (6-3)$$

The exposure time will be

$$T = \frac{E_o}{I_f} = \frac{2 E_o (\lambda f)^2}{I_s D^4}, \quad (6-4)$$

where "E_o" is the exposure required on a given film to produce some nominal amplitude transmittance change on the film. Arbitrarily define E_o as the exposure necessary to produce a 10% change in amplitude transmission. Table 3 summarizes the values of "E_o" taken from the T_A-E curves of Section 3.3.1 for the four films investigated during the program. The exposure time is also recorded in Table 3 for each film. These exposure times were calculated using Equation 6-4 and the camera parameters of Section 5:

$$\begin{aligned} \lambda &= .5 \times 10^{-3} \text{ mm} \\ D &= 15 \text{ cm} \\ f &= 1 \text{ meter} \\ \text{and } I_s &= 7 \times 10^{-15} \text{ watts/cm}^2. \end{aligned}$$

The star irradiance is for 4th magnitude stars.³⁸ Only SO-243 has a reasonable exposure time at 11.3 milliseconds.

TABLE 3 Exposures and Exposure Times for 4th Magnitude Stars

| | Exposure for 10% T _A : | Time: |
|----------------------|--------------------------------------|-------------------|
| Free Radical | 14,000 ergs/cm ² | 3.3 minutes |
| Dry Silver | 750 ergs/cm ² | 10.6 seconds |
| 649F/BIMAT (60°F) | 275 ergs/cm ² | 3.89 seconds |
| SO-243/BIMAT | 0.8 ergs/cm ² | 11.3 milliseconds |

Assumed Parameters

Diameter = 15 cm

Focal Length = 100 cm

Wavelength = $.5 \times 10^{-4}$ cm

Star Irradiance = 7×10^{-15} watts/cm²

6.2 The Maximum Exposure Due to Spacecraft Rotation

With a spinning spacecraft, the star images trace arcs on the film. These arcs can in general be correlated to yield directional information, but usually with a decreased accuracy in one direction. In any case, once the star image has moved by more than its own diameter, there is no significant increase in the local exposure of the film. The trace becomes longer, but not more dense. Thus there is a maximum possible exposure (assuming the spacecraft does not rotate more than one revolution during the exposure time.)

$$E_{\max} = I_f T \quad (6-5)$$

Where "T" is the time that the star image moves by its own diameter
or

$$T = \delta / \dot{\theta} \quad (6-6)$$

where $\dot{\theta}$ = the spacecraft rotation rate about an axis perpendicular to the camera axis.

Substituting Equations 6-6 and 6-3 into 6-5 yields

$$E_{\max} = \frac{D^3 I_s}{2 \lambda f^2 \dot{\theta}} \quad (6-7)$$

Assuming the parameters of Section 6.1 and a spin rate of 4 rpm (.42 radians/second), the maximum exposure is

$$E_{\max} = 5.6 \times 10^{-4} \text{ ergs/cm}^2$$

This exposure is quite low for the films we have been considering.

Thus even SO243 would require three orders of magnitude more exposure to produce a 10% change in amplitude transmission. In the next section we investigate whether a 10% transmission variation is necessary to produce a good correlation peak.

6.3 Increased Sensitivity by Smeared Image Integration

It is natural to ask whether integration over the smeared star images might not reduce the exposure requirements derived above. The correlation operation is a direct result of optimizing the detection process signal to noise ratio. Possibly the correlator can produce a detectable autocorrelation pulse even though the amplitude transmission variation due to each star track is much less than 10%. Many experiments have shown that correlators can detect film images which cannot be detected by other direct observations.

On the surface it might appear that correlation of a smeared star image would not increase the effective sensitivity of the film. For example, if the smeared star image is correlated with an unsmeared reference map (via the Fourier transform hologram multiplication method), then the correlation peak amplitude is not increased above the level corresponding to the maximum exposure derived in Section 6.2. This concept is sketched in Figure 16 for the academic case of a single square pulse star image. The autocorrelation of this square pulse with itself generates the triangular pulse of amplitude $A^2\delta$ shown in the upper right hand corner of Figure 16.

The second line of Figure 16 shows the image resulting from a smearing or convolution of the star image by its own length. The triangular waveshape is identical to the autocorrelation function, since convolution and correlation are identical for symmetrical functions. If this triangular pulse is correlated with the unsmeared star reference map, the pulse with amplitude $\frac{3A^3\delta^2}{4}$ is obtained. Finally, if the pulse is smeared by "N" times its own diameter, then the flat-topped correlation waveform of amplitude $A^3\delta^2$ is

Image Pulses:

Cross Correlation of Image Pulses
with Unsmearred Pulses:

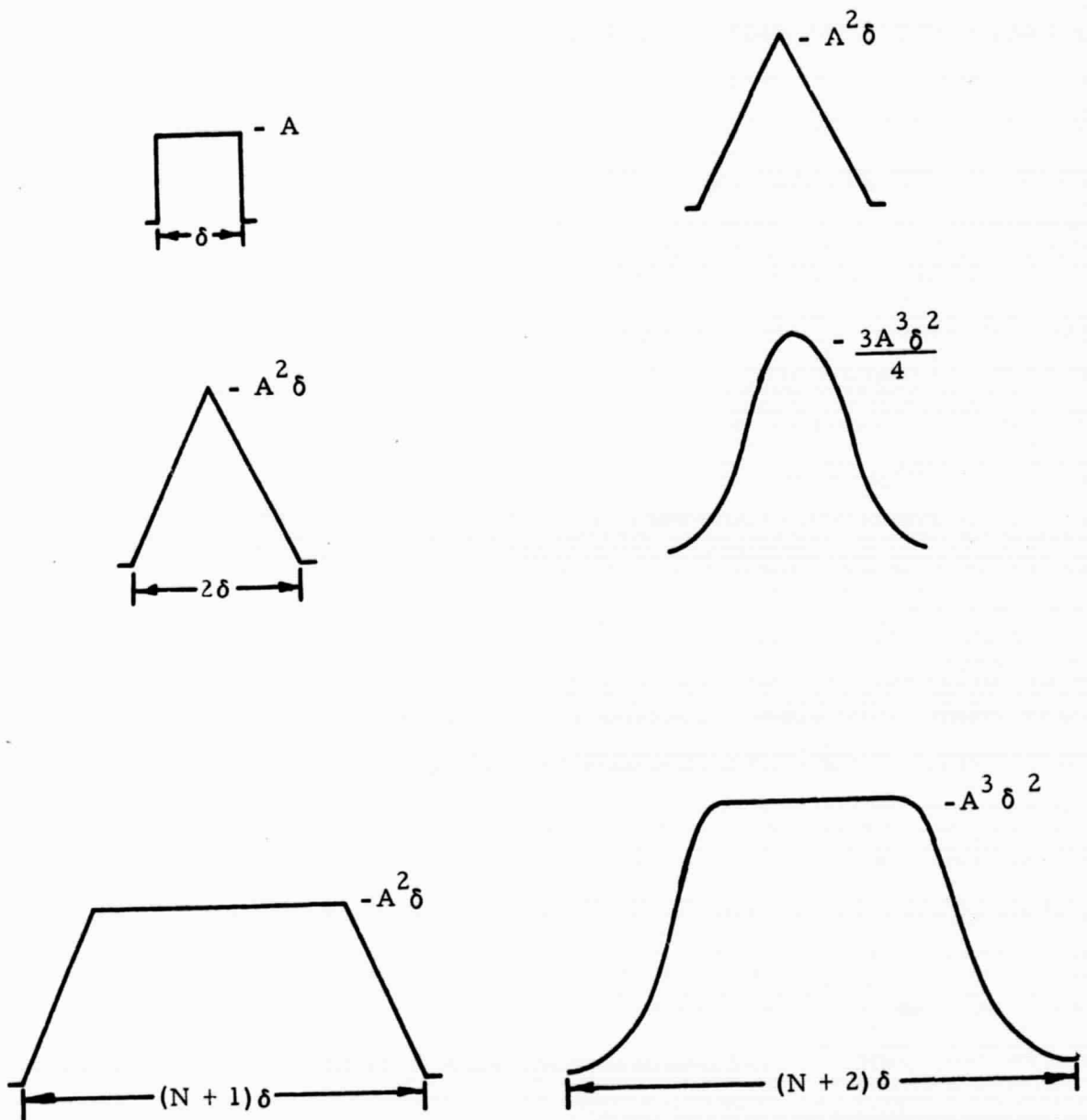


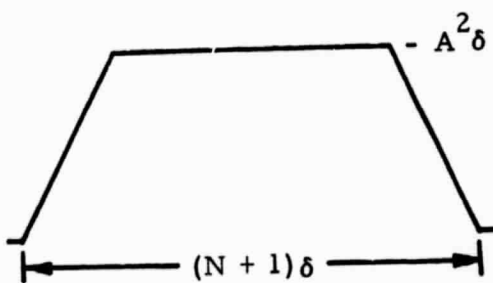
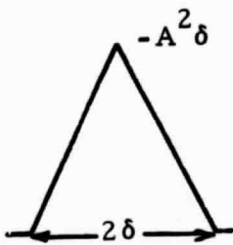
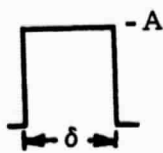
Figure 16 Smearred Star Image Pulses and Their Cross Correlations
with an Unsmearred Reference Map

obtained. The important point is that the correlation amplitude does not increase with increased smear length. However, the total energy in the correlation pulse does increase by virtue of its increased length, $(N+2)\delta$.

Ideally the reference map should be smeared by the same length as the star image prior to the production of the matched filter hologram. In this case the correlator in the spacecraft would produce autocorrelation functions. The autocorrelation pulses are sketched in Figure 17. They have sharper peaks for the two smeared cases and the amplitude of the long smeared image is proportional to "N", the number of smear diameters. These autocorrelation pulses would be easier to detect, and could be located more accurately than the pulses of Figure 16. Unfortunately, the correlator would require a very large number of reference star maps, since, for each star field of view, we would need separate holographic filters for each possible smear direction. This enormous volume of filters is in addition to the requirement of correlator rotational search which is necessary for any system. Therefore we will not consider the smeared reference map further.

Returning to the cross correlation waveforms of Figure 16, note that the total energy in the last correlation peak does increase by virtue of the increased length of the pulse. The star correlator could take advantage of this increased energy under the following circumstances: Assume a spin stabilized spacecraft with the star camera pointed perpendicular to the axis of rotation. The star tracks will be line segments across the film. The direction of these segments relative to the camera and the cross correlator is known in advance. Therefore one can fabricate a correlation detector which integrates across lines parallel to the star track lines (the correlation peak will be smeared into a line which is parallel to the star track lines). This detector

Image Pulses:



Autocorrelation Pulses:

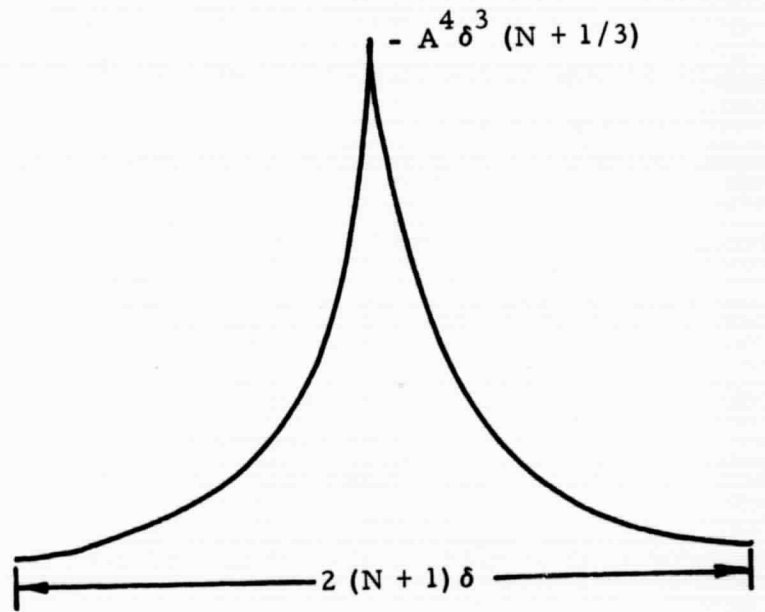
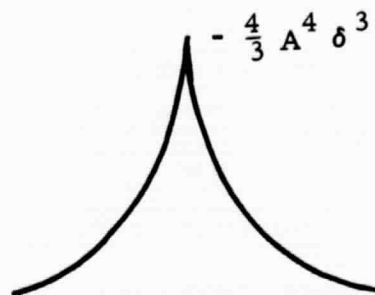
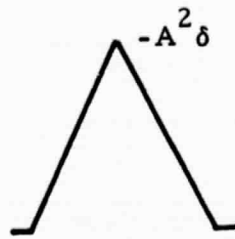


Figure 17 Autocorrelations of Smeared Pulses

might be a TV vidicon with the scan lines oriented parallel to the star track lines and an integrating video circuit. Unfortunately the vidicons or crthicons do not have adequate resolution for many applications. An alternate detection system would utilize scanning line reticles and a light detector which integrates the energy passing through a slit type opening in the reticle system.

The improvement in effective film sensitivity can be estimated by calculating the correlation signal to noise ratio as a function of the smear length. Consider a photographic film (the star image film) which is uniformly illuminated by an irradiance, I_0 . The light amplitude in the area exposed by the star image is given by

$$E_0 = \sqrt{I_0} \Delta T_A \quad (6-8)$$

where ΔT_A = the difference in amplitude transmittance in the exposed area of the film relative to the background area.

Assume that the DC light is blocked in the Fourier transform plane of the Vander Lugt type correlator. Then the light power associated with the star image is given by

$$P = \iint |F(u, v)|^2 du dv \quad (6-9)$$

$$\text{where } F(u, v) = \frac{1}{\lambda f} \iint E(x, y) \epsilon^{\frac{2\pi i}{\lambda f}(ux + vy)} dx dy \quad (6-10)$$

= The Fourier transform of the star negative amplitude function.

By Parseval's Theorem, Equation 6-9 can be written

$$P = \iint |E(x, y)|^2 dx dy \quad (6-11)$$

Since we have discrete star images, 6-11 can be approximated by a summation. The light signal power in the transform plane is therefore given approximately by

$$P \approx \sum_{i=1}^M (E_i)^2 N \delta_i^2 \quad (6-12)$$

where E_i = the light amplitude in the area of the film exposed by the "i th" star.

δ_i = the image diameter of the "i th" star

and N = the length of image smear due to spacecraft rotation; in units of star diameters.

Thus the sole effect of image motion on the signal light power in the transform plane is to linearly increase that power with smear length.

The effect of the matched filter is primarily to convert the phase of the transform light amplitude into a plane wavefront. A subsequent lens then focusses this plane wavefront to an off-axis autocorrelation peak. The filter acts as a phase corrector transmittance device. The filter is characterized mainly by its diffraction efficiency. It will generally diffract a fixed percentage of the incident transform plane light into the autocorrelation peak.

Let "C" represent the fraction of light diffracted by the matched filter into the autocorrelation peak. The light power in this peak is then given by

$$P_c \cong CN I_c \sum_{i=1}^M \Delta T_A^2 \delta_i^2 \quad (6-13)$$

If we assume "M" stars of equal irradiance and size, then

$$P_c \approx CNM \Delta T_A^2 \delta^2 I_o \quad (6-14)$$

Next estimate the film noise which will compete with this correlation signal. The light noise power at the Fourier transform plane passed by the filter is

$$P_n = I_o A_f R_n K^2 \quad (6-15)$$

where I_o = the laser irradiance incident on the film

A_f = the area of the input film

R_n = the ratio of light noise due to the film in a $(1 \text{ l/mm})^2$ area of the transform plane to the incident light.

and K^2 = the transform plane "area" in $(\text{l/mm})^2$ passed by the filter.

The average noise irradiance in the autocorrelation plane, assuming unity magnification and a diffraction efficiency of "C" as before is

$$I_n = \frac{C P_n}{A_f} = C I_o R_n K^2 \quad (6-16)$$

Assume that the matched filter is designed to pass just the main lobe of the smear star images (minus the DC peak), then

$$K^2 \approx \frac{1}{N\delta^2} \quad (6-17)$$

$$\therefore I_n = \frac{C I_o R_n}{N\delta^2} \quad (6-18)$$

The signal to noise ratio in the correlation plane can now be calculated utilizing Equations (6-14) and (6-18). If the correlation light detector integrates over an area of $N\delta^2$ corresponding to the peak, then the light noise power will be

$$P_n = I_n N\delta^2 = C I_o R_n \quad (6-19)$$

and the correlation peak signal to RMS noise ratio can be approximated by

$$\left(\frac{S}{N}\right)_c = \frac{P_c}{P_n} = \frac{NM \Delta T_A^2 \delta^2}{R_n} \quad (6-20)$$

Solving Equation (6-20) for the amplitude transmittance required we have

$$\Delta T_A^2 \geq \frac{R_n (S/N)_c}{N\delta^2 M} \quad (6-21)$$

From the film T_A -E characteristics, assume a linear relationship (small signal analysis) or

$$\Delta T_A = mE \quad (6-22)$$

But the film exposure is limited by Equation 6-7 for a spinning aircraft to

$$E_{\max} = \frac{D^3 I_s}{2 \lambda f^2 \theta} \quad (6-7)$$

Combining 6-21, 6-22 and 6-7 determines the smear length, N, and the number of stars, M, required for a given correlation signal to noise ratio:

$$NM \geq \frac{4 R_n \left(\frac{S}{N} \right)_c f^2 \theta^2}{m^2 D^4 I_s^2} \quad (6-23)$$

Since there are only 530 stars of 4th magnitude or higher³⁸, the "M" will be restricted to less than 5 or 10 for most look angles. The number of star diameters of smear can be larger, but the resolution of the correlation peak and hence the accuracy of the sensor will be degraded proportionately in one dimension.

For the camera parameters assumed earlier, and using the experimental data for BIMAT processed SO-243 film and a signal to noise ratio of 10, then the product NM must exceed 1.6×10^7 . This is based on

$$m = 1.17 \times 10^6 \text{ cm}^2/\text{joule}$$

$$\text{and } R_n = 7.5 \times 10^{-8} \text{ mm}^2$$

$$\text{and } \left(\frac{S}{N} \right)_c = 10$$

Using an image intensifier with a 500 to 1 gain, the product reduces to

$$NM \geq 64$$

and, if we assume that there are, on the average, 5 stars in the field of view, then they should be smeared by at least 13 diameters to assure adequate signal to noise ratio.

In summary, the above analysis predicts that even SO-243 type films require an image intensifier and some star image smearing to achieve adequate correlation signal to noise ratio, assuming a 4 rpm spin rate. The detected correlation peak increases linearly with smear length.

Note that the effective film sensitivity could also be increased for very stable spinning spacecraft, by multiple exposures. Once during each revolution, the star camera shutter could be opened long enough to produce the allowable star image smear length. If the spacecraft is stable, successive star tracks will be superimposed on the negative. This approach may not increase the effective sensitivity linearly due to the intermittancy effect of silver halide films, but it may be worthy of further consideration. It is also a slow process, since the exposures are accumulated at a rate of only four per minute for a 4 rpm spacecraft.

APPENDIX A
PHOTOMETRIC-RADIANT CONVERSIONS *

The sensitivities of photocathodes are published in terms of maximum radiant sensitivity, S_W^{MAX} (amp/watt) and the normalized radiant sensitivity distribution S . Phosphor data are available in terms of luminous efficiency, P_L (lumens/watt) and normalized phosphor emission spectral distribution, p . Conversions of watt-lumen-photon/sec quantities are based on the following equations:

$$\begin{aligned}
 W \text{ (watts)} &= \frac{L \text{ (lumens)} \int E(\lambda) d\lambda}{680 \int E(\lambda) V(\lambda) d\lambda} & (A-1) \\
 &= \frac{\eta \frac{\text{photons}}{\text{sec}} hc \int E(\lambda) d\lambda}{\int E(\lambda) \lambda d\lambda}
 \end{aligned}$$

where

$E(\lambda) \equiv E$ = radiant power flux (watts/unit wavelength)

$V(\lambda) = V$ = Standard visibility function (at 0.555μ
1 watt = 680 lumens)

h = Planks constant (6.624×10^{-34} joule-sec)

c = velocity of light (2.998×10^8 m/sec)

Radiant photocathode sensitivity, S_W (amp/watt)

$$= S_W^{MAX} \frac{\int ES d\lambda}{\int E d\lambda} \quad (A-2)$$

*Reference 37

Luminous photocathode sensitivity, S_L (amps/watt)

$$= \frac{S_W^{MAX} \int E S d\lambda}{680 \int E d\lambda} \quad (A-3)$$

Photocathode quantum efficiency, $S_q \left(\frac{\text{electrons}}{\text{photon}} \right)$

$$= \frac{h c S_W^{MAX} \int E S d\lambda}{e \int E \lambda d\lambda} \quad (A-4)$$

where e is the electronic charge (1.6×10^{-19} coulombs)

$$P_W \left(\frac{\text{watt}}{\text{watt}} \right) = \frac{P_L \int p d\lambda}{\int p V d\lambda} \quad (A-5)$$

$$P_q \left(\frac{\text{photons}}{\text{watt}} \right) = \frac{P_L \int p \lambda d\lambda}{680 h c \int p V d\lambda} \quad (A-6)$$

$$\text{Radiant Gain: } G_W \left(\frac{\text{watt}}{\text{watt}} \right) = S_W^{MAX} \left\{ \frac{\int E S d\lambda}{\int E d\lambda} \right\} v P_L \left\{ \frac{\int p d\lambda}{680 \int p V d\lambda} \right\} \quad (A-7)$$

$$\text{Luminous Gain: } G_L \left(\frac{\text{lumen}}{\text{lumen}} \right) = S_W^{MAX} \left\{ \frac{\int E S d\lambda}{680 \int E V d\lambda} \right\} v P_L \quad (A-8)$$

$$\text{Photon Gain: } G_P \left(\frac{\text{photon}}{\text{photon}} \right) = S_W^{MAX} \left\{ \frac{\int E S d\lambda}{\int E \lambda d\lambda} \right\} \frac{v P_L}{680} \left\{ \frac{\int p \lambda d\lambda}{\int p V d\lambda} \right\} \quad (A-9)$$

Note if $E = p$ (same input and output light distribution) we obtain the following relationship

$$G_W = G_L = G_{LW} = \frac{S_W^{MAX} v P_L}{680} \left\{ \frac{\int p S d\lambda}{\int p V d\lambda} \right\} \quad (A-10)$$

The product of

$$(n/L) S_q = \frac{S_W^{MAX}}{e} \left\{ \frac{\int E S d\lambda}{680 \int E V d\lambda} \right\} = \left(\frac{\text{photoelectrons}}{\text{lumen sec}} \right) \quad (A-10)$$

is useful in calculating the photoelectron emission due to one foot candle illumination. Conversions of S or G values for light distribution E_1 to a light distribution E can be accomplished using the equations below:

$$\frac{G_W(E)}{G_W(E_1)} = \frac{S_W(E)}{S_W(E_1)} = \frac{\int E S d\lambda}{\int E_1 S d\lambda} = \frac{\int E_1 d\lambda}{\int E d\lambda} \quad (A-11)$$

$$\frac{G_L(E)}{G_L(E_1)} = \frac{S_L(E)}{S_L(E_1)} = \frac{\int E S d\lambda}{\int E_1 S d\lambda} = \frac{\int E_1 V d\lambda}{\int E V d\lambda} \quad (A-12)$$

$$\frac{G_g(E)}{G_g(E_1)} = \frac{S_y(E)}{S_g(E_1)} = \frac{\int E S d\lambda}{\int E_1 S d\lambda} = \frac{\int E_1 \lambda d\lambda}{\int E \lambda d\lambda} \quad (A-13)$$

For a given input E, the relative response of two photosurfaces S_a and S_b and hence G_a and G_b (regardless of whether they are luminous, radiant, or quantum figures of merit) is

$$\frac{G(S_a)}{G(S_b)} = \frac{S_a}{S_b} = \frac{S_{W,a}^{MAX} \int E S_a d\lambda}{S_{W,b}^{MAX} \int E S_b d\lambda} \quad (A-14)$$

All integrals are evaluated between 0 and ∞ .

The calculation of maximum radiant figures of merit can be obtained by replacing all normalizing integrals by unity and using the maximum radiant values and taking the proper correction terms from the visibility curve for the particular wavelength value.

APPENDIX B
DETECTIVE QUANTUM EFFICIENCY
OF PHOTOGRAPHIC FILMS

If we consider the energy received by a detector per unit time from a faint object as a signal, and the night skylight (any ambient light source) as noise power which tends to obscure the signal, we typically define a signal-to-noise ratio (SNR) which describes the information content incident on the recording system. Now defining n_s as the combined number of photons received from an object and the night sky background per unit time per unit area (photo flux density) and n_b as the average number of photons per unit time per unit area received from the sky background alone (noise). The signal is defined as

$$S = (n_s - n_b) A t \quad (B-1)$$

where A is the area of the detector receiving the information during an integration or detector time t . Since the input fluctuations follow a Poisson distribution, the expression for the noise is given by

$$N = (n_b A t)^{1/2} \quad (B-2)$$

Combining the above equations the expression for the input signal-to-noise is given by

$$S/N = [(n_s - n_b)(A t)^{1/2}] (n_b)^{-1/2} \quad (B-3)$$

Typically the term "quantum efficiency" has always been defined as the ratio of the numbers of two countable events. This type of quantum efficiency is called the "responsive" quantum efficiency and is defined as the ratio of the number of countable output events to the number of photons that act on the device³⁵. Our primary concern in this report, however, is with what has been defined as the "detective" quantum efficiency³⁶. The detective quantum efficiency is formulated in terms of the detecting ability of a detector in which a steady ambient radiation is present in addition to the signal. The importance of this concept depends on whether the noise due to the ambient radiation is dominant over other noise sources of the detector. This condition is almost always satisfied in the use of photographic films, multiplier phototubes, image intensifiers and combinations of the above devices.

Since the process of photometry (radiometry) involves some type of detector or counter, the accuracy of the photometric measurement is established not by the number of photons incident upon the detector, but by the number which are actually utilized by the detector. If the number of photons utilized by the detector is less than the number of photons incident (as in the case with film), the signal to noise ratio in the output of the detector $(S/N)_{out}$ will be less than $(S/N)_{in}$. Thus the $(S/N)_{out}$ is the quantity which ultimately establishes the accuracy of the measurement and it is therefore desirable to operate in a way such as to maximize the $(S/N)_{out}$.

The detective quantum efficiency is defined as

$$Q = \frac{(S/N)_{out}^2}{(S/N)_{in}^2} \quad (B-4)$$

The reason for the second power of the ratio of the signal to noise ratios is that for an ideal detector the responsive and detective quantum efficiency (DQE) are equal if and only if a second power relationship is used. We can now rearrange equation (B-4) and obtain the expression for the $(S/N)_{out}$ as shown

$$(S/N)_{out} = Q^{1/2} (S/N)_{in} \quad (B-5)$$

It is readily apparent that this function is a measure of the efficiency with which a detector transduces information. In this form the relationship is useful for any detector, photographic or photoelectric, since it relates the input and output signal-to-noise ratios. If Q is measured in specific parameters associated with photographic films, then we can predict the optimum recording parameters to maximize the sensitivity and response of the film detector for a given application.

Photographic negatives have a characteristic which sets them off from other detectors, namely their ability to integrate radiation that falls on the detector over a period of time. With most detectors the only ambient radiation that is relevant is the radiation that falls on the detector simultaneously with the signal. But with photographic films the ambient radiation may precede or follow the signal radiation. Thus it is often convenient to refer to the ambient radiation as the "pre-exposure". As we will see the DQE is a function of the pre-exposure. Qualitatively the reason for this dependence is as follows:

In order for a photographic grain to become developable, the grain must be acted on by a number of photons, of order of magnitude 10; at exposures less than the DQE_{\max} a large majority of the incident photons are wasted on grains that receive less than the necessary number to become developable. Conversely, for exposures much greater than that of the maximum, a large majority of the incident photons are wasted on grains that have already received a number sufficient to make them developable. Thus at some intermediate exposure corresponding to the $(DQE)_{\max}$, there is a point where these two tendencies are balanced.

The detective quantum efficiency of a given photographic film depends on the following:

1. The amount of ambient exposure
2. The spectral distribution of the radiation signal
3. The development procedure.

The noise in photographic negatives arises from the density fluctuations. If one measures the density in an aperture at a large number of different places, the measured densities will not be all the same. The set of measured densities may be characterized by a mean density that will be denoted \bar{D} and by a root-means-square deviation from \bar{D} , denoted by σ_D . Thus the output signal-to-noise in photographic film is given by

$$(S/N)_{\text{out}} = \bar{D} / \sigma_D \quad (\text{B-6})$$

where $D = D_s - D_b = G(n_s - n_b)t$

where G is the slope of the density vs log exposure curve. Using the relationships developed previously the DQE is given by

$$Q = (h^2 G^2 / A \sigma_D^2) (n_b t)^{-1} \quad (\text{B-7})$$

where $G = dD/d [\log (n_b t)] = \text{Gamma of the film}$

$$h = \log e$$

Figure B-1 shows a typical D vs $\log E$ and DQE plotted on the same graph demonstrating the existence of a maximum as explained previously.

Thus the DQE is one of the best single measures of the detecting ability of a photographic film since it combines film speed, gamma, and and granularity as a figure of merit. One aspect it fails to specify is the important limitation of light scattering in the emulsion which limits resolution. Separate experimental measurements are required to ascertain this effect for various films.

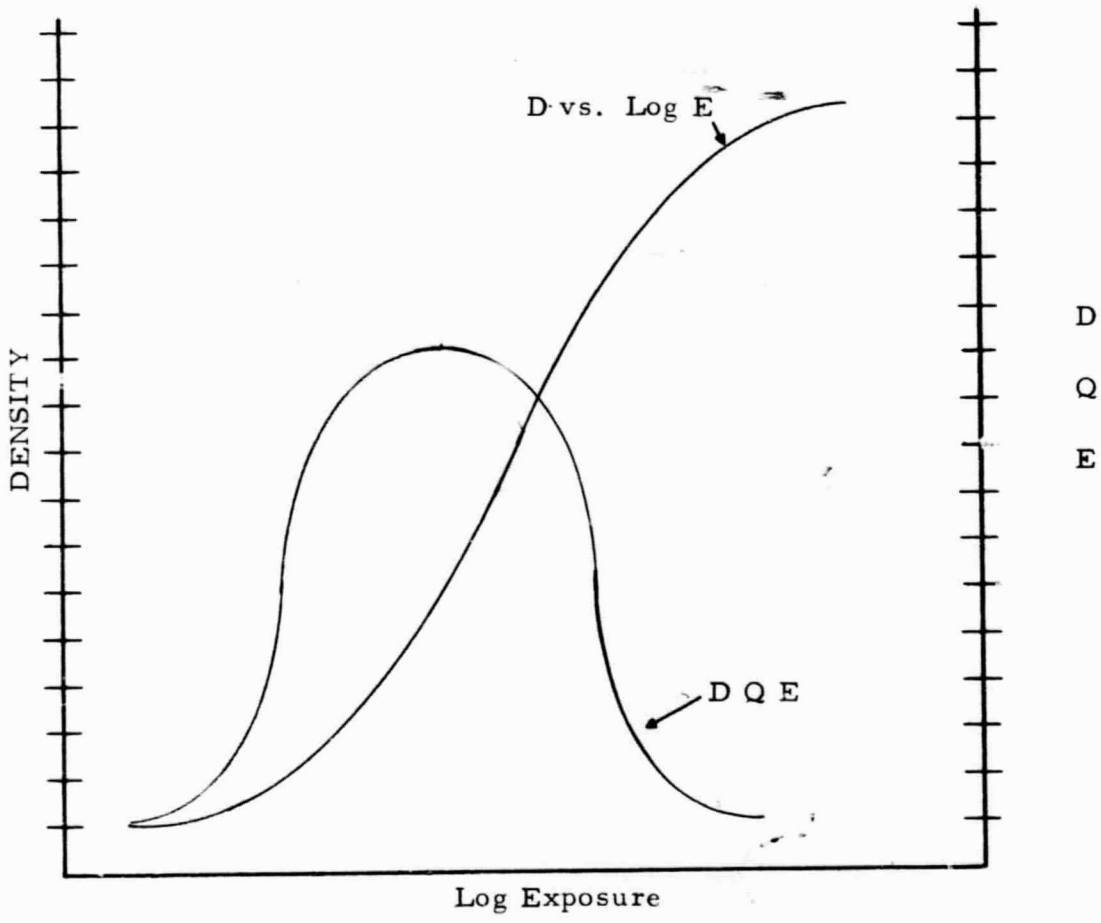


Figure B-1 DQE as a Function of the Log Exposure

Addresses of Film Suppliers

1 Free Radical Film

Photohorizons, a Division of Horizons Research, Inc.
23300 Mercantile Road
Cleveland, Ohio
44122
(216) 464-1942

2) Dry Silver Film

The 3M Company
3M Center
St. Paul, Minnesota
55101
(612) 733-1110

3) BIMAT Diffusion Transfer Processing[®] Film

Mark Systems, Inc.
10950 North Tantau Avenue
Cupertino, California
95014
(408) 253-8300

REFERENCES

1. Manual of Physical Properties of Kodak Aerial and Special Sensitized Materials, Eastman Kodak Publication No. M-118, October 1968
2. R. G. Tarkington, "The Kodak Bimat Process," presented at the 30th Annual Meeting of the American Society of Photogrammetry, Washington, D.C., March 15-21, 1964.
3. Private Communication with Richard A. Fotland of Horizons Research.
4. H. M. Smith, "Photographic Relief Images," J. Opt. Soc. Am., 58, 533 (1968)
5. Techniques of Microphotography, Eastman Kodak Publication P-52, November 1964
6. Richard A. Fotland, "Optically Developed Free-Radical Photosensitive Materials", Symposium on Non-Silver Photographic Processes, Organized by the Science Committee of the Royal Photographic Society, 30 September to 30 October 1969, Oxford.
7. R. H. Sprague and H. L. Fichter, Photo.Sci.Eng. 8:(2), 95(1964).
8. L. F. Herk and F. A. Hamm, "An Evaluation of Dry Silver Laser Beam Recording Films," Third Annual Wideband Analog Recording Symposium, RADC-TR-69-377, Volume 1, October 1969.
9. U.S. Patent 2, 352, 014 (1941)
10. Private Communication with Franklin K. H. Ching of Mark Systems, January 30, 1970.

11. L. W. Tregillus, "A Diffusion - Transfer Web-Process", presented at the Society of Photographic Scientists and Engineers, Boston Meeting, May 7-11, 1962.
12. L. W. Tregillus, "Image Characteristics in Kodak Bimat Transfer Film Processing, I. Grain Structure," J. Photo.Sci., 15, 45(1967)
13. L. W. Tregillus, "Image Characteristics in Kodak Bimat Transfer Film Processing II. Image Structure," J. Photo.Sci., 15, 126 (1967)
14. See "Quality Considerations of Diffusion Transfer Processing" Eastman Kodak Tech Bits, No. 1, 1969.
15. Private Communication with Ed Turk of Eastman Kodak, October 20, 1969.
16. N. J. Harrick, Internal Reflection Spectroscopy, Interscience Publishers, 1967
17. C. E. Thomas, "Coherent Optical Noise Suppression," Applied Optics, 7, 517, (1968)
18. Kodak Plates and Films for Science and Industry, Eastman Kodak Publication P-9, January, 1967.
19. Lewis & James, Photo.Sci. Eng. 13, 54, (1969)
20. Schagen, P., Brunning, H., and Francken, J. C., Philips Res. Rep. 7/2, 1952, p. 119.
21. Storidenheimer, R. G., Moor, J. C., "A Developmental Two-Stage Image Intensifier" Image Intensifier Symposium Proceeding, 1958.
22. Kapany, N. S., and Capellaro, D. F., J. Opt. Soc. Am., 51, 23 (1961)

23. Potter, R. J., "Transmission Properties of Optical Fibers," Mtg. Opt. Soc. Am., Ottawa, 1959.
24. Babcock, H. W. Johnson, J. J., Astrophysics, 44, 271 (1941)
p. 271.
25. Hiltner, W. A. and Niklas, W. F., "A Low Background Image Tube for Electronography," 2nd Symp., Photo. El. Image Dev., London, 1961.
26. Fried, D. L., Applied Optics, 4, 79,(1965)
27. Lallemand, A., Comptes Rendus, 203, 243 (1936)
28. Webb, J. H., J. Opt. Soc. Am., 38, 312 (1948)
29. Hiltner, W. A., "Image Converters with Protecting Foils"
Image Intensifier Symposium Proceedings, 1958
30. Vernier, P. Bull. Astr., 83 (1959)
31. Hiltner, W. A., "Design and Performance of an Image Intensifier for Astronomical Application", Image Intensifier Symposium, 1961.
32. Private Communication, Dr. Walter Roth, KMSTC, San Diego, Calif.
33. Jones, R. C., "Minimum Energy Detectable by Films", PhotoSci. Eng. 2, 198 (1958)
34. Marchant, J. C., Millikan, A. G., "Photographic Detection of Fading Stellar Objects", J. Opt. Soc. Am., 55, 907,(1965)

35. Jones, R. C., "On the Quantum Efficiency of Photographic Negatives", Photo. Sci. Eng., 2 (1958)
36. Rose, A., Advances in Electronics Academic Press, New York 1948
37. Dolon, P. J., Niklas, W. F., "Gain and Resolution of Fiber Optic Intensifier", Image Intensifier Symposium, 1961.
38. Kauth, R. "Backgrounds", Handbook of Military Infrared Technology, Office of Naval Research, Department of the Navy, Washington, D. C. 1965.